

# Testing Gravitational-Wave Signal From Verification Binaries with Space-Based Gravitational-Wave Detectors

Zi-Heng Yu,<sup>1,\*</sup> Sen Yang,<sup>1,\*</sup> Liangliang Ren,<sup>2</sup> and Shun-Jia Huang<sup>1,†</sup>

<sup>1</sup>*School of Science, Shenzhen Campus of Sun Yat-sen University, Shenzhen 518107, China*

<sup>2</sup>*School of Electrical and Electronic Engineering, Anhui Science and Technology University, Bengbu, Anhui 233030, China*

(Dated: March 3, 2026)

Space-based gravitational wave (GW) detectors will open the millihertz band to survey ultra-compact binaries (UCBs). *Verification binaries* (VBs) is a key to verifying the performance of space-based GW detectors because its parameters are known from electromagnetic observations and it is expected to be a detectable source of GW. We evaluated 73 VBs, computing their detection prospects and parameter estimation precision for individual GW detectors and networks. Among single detectors, DECIGO shows the highest sensitivity, detecting 71 sources at signal-to-noise ratio  $\rho \geq 5$ , compared to 42 for LISA, 32 for Taiji, and 27 for TianQin, while the full TianQin + LISA + Taiji + DECIGO network improves this to 73 detectable sources. For parameter estimation, individual detectors achieve median precisions on the order of  $\sim 10^{-2} - 10^{-1} M_{\odot}$  for chirp mass,  $\sim 1$  kpc for distance,  $\sim 1 - 17$  deg for inclination and  $\sim 10^{-4} - 10^{-2} \text{ deg}^2$  for sky localization. The complete TianQin + LISA + Taiji + DECIGO network enhances these constraints substantially, reducing the median uncertainties to approximately  $\sim 10^{-2} M_{\odot}$  in chirp mass,  $\sim 10^{-2}$  kpc in distance,  $\sim 1$  deg in inclination and  $\sim 10^{-4} \text{ deg}^2$  in sky localization. The upcoming space-based GW detectors, especially their networks, have outstanding observational capabilities for UCB, which will advance our research on multi-messenger astronomy and deepen our understanding of UCB in the Milky Way.

## I. INTRODUCTION

In 1916, based on general relativity (GR), Albert Einstein predicted the existence of GWs [1]. GWs propagate the perturbations of spacetime curvature, radiating outward at the speed of light. These waves convey energy and angular momentum, and critically encode detailed astrophysical information regarding the dynamics of their sources [2, 3]. As such, they constitute a qualitatively new messenger, distinct from and complementary to electromagnetic (EM) radiation [4]. Currently, the prevailing detection modality is laser interferometry [5–7], specifically the Michelson interferometric architecture.

In 2015, Advanced LIGO (aLIGO) [5] made the first direct detection of GW (GW150914) [8], initiating a new era in GW astronomy. In the following years, Advanced Virgo (aVirgo) [6] and KAGRA [9] also operated successively to detect GW signals, forming the LIGO-Virgo-KAGRA (LVK) detection network together with aLIGO. So far, LVK has detected  $\sim 90$  GW events [10–15], which made the GW observation a new window to understanding the Universe.

Ground-based interferometers such as aLIGO and aVirgo are sensitive only to the 10 Hz–kHz band [16], but GW span many orders of magnitude in frequency, requiring complementary facilities: the cosmic microwave background polarization experiments for femtohertz [17], pulsar-timing arrays for nanohertz [18, 19], and space-based laser interferometers for millihertz [20, 21]. The

millihertz band hosts the most diverse population: massive black-hole binaries ( $10^3 - 10^7 M_{\odot}$ ) from galaxy mergers [22–24], extreme-mass-ratio inspirals (EMRIs) [25, 26], and UCBs of white dwarfs (WDs), neutron stars, and stellar-mass black holes [27–30], together with astrophysical and cosmological stochastic backgrounds [31], thus bridging astronomy and fundamental physics [32, 33]. Among these GW sources, UCBs have the highest detectable quantity, and space-based laser interferometers are expected to capture tens of thousands of UCBs [28, 34–36].

If GW detectors can also detect the GW signals radiated by UCBs that EM telescopes have observed, scientists can use such sources, the so-called *verification binaries* (VBs), to calibrate the instrument noise of GW detectors themselves. In 2006, A. Stroeer and A. Vecchio et al. [37] performed a comprehensive parameter analysis of 30 verification-binary candidates, focusing on the signal-to-noise ratios (SNRs) expected for these systems. They concluded that RX J0806.3+1527, V407 Vul, ES Cet, and AM CVn satisfy the criteria for classification as reliable VBs. In 2018, Kupfer et al. [38] computed the SNRs of approximately fifty VBs using parallaxes from Gaia Data Release 2. For the systems exhibiting high SNRs, they employed Fisher information matrix (FIM) formalism to forecast the parameters uncertainty on the GW amplitude ( $\mathcal{A}$ ) and the inclination angle ( $\iota$ ). In 2020, Shun-Jia Huang et al. [36] investigated the detection prospects for Galactic double white dwarf binaries (DWDs) with the space-borne GW observatory TianQin. They concluded that TianQin is expected to resolve 12 of the  $\sim 100$  DWDs already identified in the Galaxy, and TianQin could expand the DWD catalogue to approximately  $10^4$ . The authors further emphasized the scientific benefits of coordinated multi-messenger campaigns combining

\* These authors contributed equally to this work and should be considered co-first authors.

† corresponding author: huangshj69@sysu.edu.cn

TianQin data with EM facilities.

Building on previous research, this paper updates the VB catalogue and analyzes the detection capabilities of the individual space-based GW detectors and joint detection by multiple detectors. In Section II, we outline the sample of the currently known VB. In Section III, we derive formulas for computing the SNR and uncertainties on binary parameters. In Section IV, we calculate the detection numbers and parameter estimation of nine configurations involving four individual detectors and five detector networks for VBs. Finally, we summarize our main findings in Section V.

## II. VERIFICATION BINARIES

We assembled a sample of five classes of VB systems: DWDs, AM Canum Venaticorum binaries (AM CVns), close white dwarf binaries (CWDBs), ultra-compact X-ray binaries (UCXBs) and Subdwarf binaries (sdBs).

DWDs constitute the most abundant class of UCBs in the Milky Way. They are expected to be the principal contributor to the signals detected by space-based GW detector [39]. Millions of DWDs radiate low-frequency GWs signals, merging into an irresolvable background noise or the galactic background. In contrast, the louder, individually resolvable sources emerge above this confusion limit; together with high-frequency sources, these objects constitute a population of  $\sim 10^4$  detectable white-dwarf binaries [34, 35]. DWDs can be assembled from helium-core, carbon/oxygen-core, or oxygen/neon/magnesium-core WDss in any combination, with a combined mass typically below  $1.4 M_{\odot}$  [40].

AM CVns, which originate from DWDs, consist of a WD accreting matter from a hydrogen-deficient star or WD companion [41, 42]. AM CVns are of great value to space-based GW detectors, as they deliver multi-band EM information and their GW frequencies fall mainly within the space-based GW detectors sensitive band [43]. Typical AM CVn systems such as J0806, V407 Vul and ES Cet have been highlighted as important verification sources for space-based GW detectors (e.g. [36, 38]).

CWDBs are compact binary systems in which at least one component is a WD. They are an important branch of the evolution channel of main-sequence (MS) star binaries. Depending on the component type and the mass-transfer status, CWDBs are usually divided into three main classes: post-common-envelope binaries, detached systems composed of a WD and a MS star [44, 45]; cataclysmic variables, semi-detached systems in which a low-mass donor fills its Roche lobe and transfers matter to the WD [46]; and DWDs, detached pairs of two WDs that are the end products of two successive common-envelope phases [34]. The orbital periods of CWDBs range from a few minutes to a day, with the shortest-period objects ( $P_{\text{orb}} \lesssim 60$  min) being the most potential individually resolvable GW sources for millihertz GW detectors such as LISA and TianQin [44]. ZTF J052610.40+593445.85

is a CWDB with shortest orbital period of 20.5 minutes and constitutes a potentially detectable millihertz GW source [44].

UCXBs comprise a neutron star or stellar-mass black hole plus a donor star, with typical orbital periods of less than 60 min [47, 48]. The compactness of UCXB confines the donor to be WD, semi-degenerate dwarf, or helium star [47]. UCXBs are also important GW sources. 1RXS J171824.2-402934 ( $P_{\text{orb}} \sim 7.0$  min), 4U 1820-30 ( $P_{\text{orb}} \sim 11.4$  min) and 4U 0513-40 ( $P_{\text{orb}} \sim 16.9$  min) are all candidate sources within the millihertz band of space-based detectors [49–51].

sdBs contain a subdwarf B star together with a compact companion, a WD or neutron star. Angular-momentum loss via GW combined with magnetic braking shrinks the orbit further, leading a sdB to a UCXB or a millisecond-pulsar binary [40]. The most compact sdBs attain orbital periods  $P_{\text{orb}} \lesssim 1$  hour [52–55], which makes them potential detectable sources. OW J0741 ( $P_{\text{orb}} \sim 45.0$  min), CD-30 11223 ( $P_{\text{orb}} \sim 70.9$  min) and HD 265435 ( $P_{\text{orb}} \sim 99.1$  min) are sdBs whose orbital frequencies fall in the millihertz band. They are potential detected by the space-based GW detectors [53, 54, 56].

We have collected the currently known candidates of these five VB types and recorded their measured and estimated GW parameters in Table III. This source table includes 19 AM CVns, 34 DWDs, 13 CWDBs, 3 UCXBs and 3 sdBs.

## III. MODELING SIGNAL AND NOISE

### A. Gravitational wave signal from a single binary

For each binary, it can be described by the following parameters: orbital period  $P$ , component masses  $m_1$  and  $m_2$ , the ecliptic latitude  $\lambda$  and longitude  $\beta$ , distance from the Sun  $d$ , inclination angle  $\iota$ , polarization angle  $\psi_S$ , and the initial orbital phase  $\phi_0$ .

For binaries whose frequencies are significantly smaller than the mission lifetime of many detectors of several years, they can be safely considered as monochromatic sources, meaning that the GWs generated by them can be described by a set of seven parameters: the dimensionless amplitude  $\mathcal{A}$ , GW frequency  $f = 2/P$ ,  $\lambda$ ,  $\beta$ ,  $\iota$ ,  $\psi_S$ , and  $\phi_0$ .

From the quadrupole formula of GW, the waveforms of the plus  $+$  and cross  $\times$  modes in the principal polarization coordinate are given [57, 58]

$$h_+(t) = \mathcal{A}(1 + \cos^2 \iota) \cos(2\pi ft + \phi_0 + \Phi_D(t)), \quad (1)$$

$$h_{\times}(t) = 2\mathcal{A} \cos \iota \sin(2\pi ft + \phi_0 + \Phi_D(t)), \quad (2)$$

with

$$\mathcal{A} = \frac{2(G\mathcal{M})^{5/3}}{c^4 d} (\pi f)^{2/3}, \quad (3)$$

where  $\mathcal{M} \equiv (m_1 m_2)^{3/5} / (m_1 + m_2)^{1/5}$  is the chirp mass, and  $G$  and  $c$  are the gravitational constant and the speed of light, respectively. The additional term  $\Phi_D(t)$  in the GW phase [Eq. (1)-(2)] is the Doppler phase arising from the periodic motion of detector around the Sun:

$$\Phi_D(t) = 2\pi f t \frac{R}{c} \sin(\pi/2 - \beta) \cos(2\pi f_m t - \lambda), \quad (4)$$

where  $R = 1\text{A.U.}$  is the distance between the Earth and the Sun, and  $f_m = 1/\text{year}$  is the modulation frequency.

## B. Detector response

The prevailing space-based GW detectors envision a unit of three drag-free satellites orbiting the Earth or the Sun. Satellites will form an equilateral triangle unit oriented in such a way that the normal vector to the detector's plane is pointing towards a specific source or cyclic.

The triangle unit can be regarded as the two Michelson interferometers 1 and 2. For each interferometer, it can record the GW strain as the detector [59]:

$$h(t) = h_+(t)F^+(t, \theta_S, \phi_S, \psi_S) + h_\times(t)F^\times(t, \theta_S, \phi_S, \psi_S), \quad (5)$$

here  $F_{+, \times}$  are the antenna pattern functions.  $(\theta_S, \phi_S)$  is the latitude and longitude of the source in the detector's coordinate frame. The antenna pattern functions can be written as follows:

$$F_1^+(t, \theta_S, \phi_S, \psi_S) = \frac{\sqrt{3}}{2} \left( \frac{1}{2} (1 + \cos^2 \theta_S) \cos 2\phi_S(t) \cos 2\psi_S - \cos \theta_S \sin 2\phi_S(t) \sin 2\psi_S \right), \quad (6)$$

$$F_1^\times(t, \theta_S, \phi_S, \psi_S) = \frac{\sqrt{3}}{2} \left( \frac{1}{2} (1 + \cos^2 \theta_S) \cos 2\phi_S(t) \sin 2\psi_S + \cos \theta_S \sin 2\phi_S(t) \cos 2\psi_S \right), \quad (7)$$

$$F_2^+(t, \theta_S, \phi_S, \psi_S) = F_1^+(t, \theta_S, \phi_S - \frac{\pi}{4}, \psi_S), \quad (8)$$

$$F_2^\times(t, \theta_S, \phi_S, \psi_S) = F_1^\times(t, \theta_S, \phi_S - \frac{\pi}{4}, \psi_S), \quad (9)$$

where subscripts 1 and 2 are labels for the two Michelson signals, as indicated by the  $\pi/4$  phase difference between the corresponding antenna pattern functions [59]. Note that there is a coefficient  $\sqrt{3}/2$  in response calculation when considering the  $60^\circ$ -interferometers as L-shaped interferometers.

## C. Sensitivity curve

In GW detection, a key performance metric of the detectors is their frequencies response to signal sources, which is characterized by the detector's sensitivity curve. This curve describes the detector's sensitivity across different frequencies and is closely related to the noise power spectral density (PSD).

The sensitivity curve of TianQin is given by [36]

$$S_n^{\text{TQ}}(f) = \frac{1}{L^2} \left[ \frac{4S_a}{(2\pi f)^4} \left( 1 + \frac{10^{-4}\text{Hz}}{f} \right) + S_x \right] \times \left[ 1 + 0.6 \left( \frac{f}{f_*} \right) \right], \quad (10)$$

where transfer frequency  $f_* = \frac{c}{2\pi L}$ , arm length  $L$ , acceleration noise  $S_a$ , and displacement measurement noise  $S_x$  are given in Table I.

For both LISA and Taiji, they share an identical sensitivity curve of the form as [60, 61]

$$S_n^{\text{LISA}}, S_n^{\text{Taiji}}(f) = \frac{1}{L^2} \left[ \frac{4S_a}{(2\pi f)^4} \left( 1 + \frac{4 \times 10^{-4}\text{Hz}}{f} \right) \left( 1 + \left( \frac{f}{8 \times 10^{-3}} \right)^4 \right) + S_x \right] \times \left[ 1 + 0.6 \left( \frac{f}{f_*} \right) \right] + S_{conf}^{\text{LISA, Taiji}}, \quad (11)$$

where  $L, S_a, S_x$  are similarly given in Table I.

While LISA and Taiji will resolve individual signals well, there are still a large number of faint signals from galactic DWD systems that are not strong enough to be identified individually. The GWs from these sources will form a significant foreground confusion noise for the sub-mHz observation, which can be characterized by its PSD  $S_{conf}(f)$ , being given by

$$S_{conf}^{\text{LISA}}(f) = \frac{3}{10} \times 9 \times 10^{-45} \times f^{-7/3} \times \exp(-f^{0.138} - 221 \times f \times \sin(521 \times f)) \times (1 + \tanh(1680 \times (0.00113 - f))), \quad (12)$$

$$S_{conf}^{\text{Taiji}}(f) = \exp \left( \sum_{i=0}^5 a_i \left( \ln \left( \frac{f}{\text{mHz}} \right) \right)^i \right), \quad (13)$$

where  $a_i$  are the coefficients of polynomial, given in Table II.

For DECIGO, its sensitivity curve can be expressed as [62]

$$S_n^{\text{DECIGO}}(f) = \frac{1}{L^2} \left[ \frac{4S_a}{(2\pi f)^4} + S_x \left( 1 + \left( \frac{f}{f_p} \right)^2 \right) + \frac{S_r}{(2\pi f)^4} \left( \frac{1}{1 + \left( \frac{f}{f_p} \right)^2} \right) \right], \quad (14)$$

where  $f_p = 7.36$  Hz,  $S_a, S_x$ , radiation noise  $S_r$  are given in Table I.

All the sensitivity curves illustrated above with their foreground confusion noise are represented in Fig. 1. This figure clearly delineates the frequency-dependent sensitivity of each detector, with DECIGO demonstrating the lowest noise floor across nearly the entire millihertz band, highlighting its superior design sensitivity.

TABLE I. Key parameters for the configurations of TianQin, LISA, Taiji and DECIGO.

Parameters	TianQin	LISA	Taiji	DECIGO
Number of satellites	N=3	N=3	N=3	N=4 × 3=12
Orientation	$\lambda = 120.4^\circ, \beta = -4.7^\circ$	cyclic	cyclic	cyclic
Duty cycle	50%	75%	75%	75%
Mission lifetime (yr)	5	4	4	4
Arm length $L$ (m)	$\sqrt{3} \times 10^8$	$2.5 \times 10^9$	$3 \times 10^9$	$1 \times 10^6$
Displacement measurement noise $S_x$ ( $\text{m}^2\text{Hz}^{-1}$ )	$1 \times 10^{-24}$	$2.25 \times 10^{-22}$	$6.4 \times 10^{-23}$	$7.05 \times 10^{-36}$
Acceleration noise $S_a$ ( $\text{m}^2\text{s}^{-4}\text{Hz}^{-1}$ )	$1 \times 10^{-30}$	$9 \times 10^{-30}$	$9 \times 10^{-30}$	$2.15 \times 10^{-37}$
Radiation pressure noise $S_r$ ( $\text{m}^2\text{s}^{-4}\text{Hz}^{-1}$ )	–	–	–	$7.48 \times 10^{-36}$

TABLE II. The fitted coefficients of the galactic foreground spectra for Taiji

Parameter	Taiji
$a_0$	-85.5448
$a_1$	-3.23671
$a_2$	-1.64187
$a_3$	-1.14711
$a_4$	0.0325887
$a_5$	0.187854

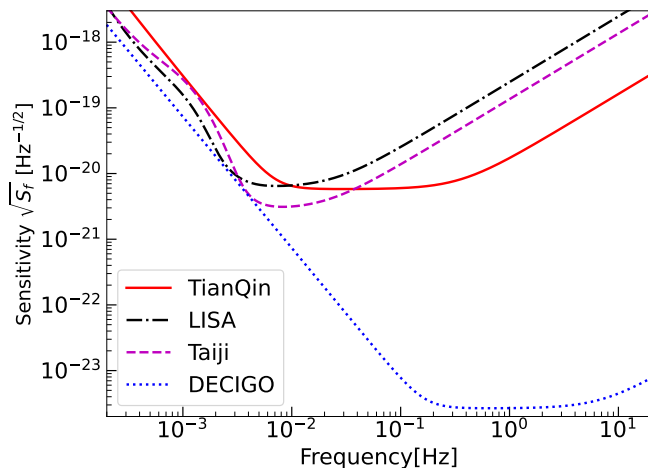


FIG. 1. The sensitivity curves of TianQin, LISA, Taiji and DECIGO. The red solid line, black dash-dot line, magenta dashed line, and blue dotted line correspond to TianQin, LISA, Taiji, and DECIGO respectively, defined in Eqs. (10)-(14).

TianQin exhibits a comparable shape to LISA and Taiji but with a lower noise level above approximately 40 mHz, consistent with its shorter arm length. All curves exhibit a characteristic rise at low frequencies due to acceleration noise, while at high frequencies they gradually increase as the transfer frequency term dominates. Notably, the Galactic foreground confusion noise creates a “bump” in the LISA and Taiji curves below a few millihertz, representing the unresolved GWs from millions of DWDs in the Milky Way.

#### D. Signal to noise ratio

The SNR  $\rho$  of a signal is defined as

$$\rho^2 = (h|h), \quad (15)$$

where the inner product  $(\cdot|\cdot)$  is defined as

$$\begin{aligned} (a|b) &= 4\Re \int_0^\infty df \frac{\tilde{a}^*(f)\tilde{b}(f)}{S_n(f)} \\ &\simeq \frac{2}{S_n(f_0)} \int_0^T dt a(t)b(t), \end{aligned} \quad (16)$$

where  $\tilde{a}(f)$  and  $\tilde{b}(f)$  are the Fourier transformations of two generic functions  $a(t)$  and  $b(t)$ ,  $S_n(f)$  is the sensitivity curve of detector.

Therefore, the SNR for a single binary can be calculated as

$$\rho^2 = (h|h) \simeq \frac{2}{S_n(f_0)} \int_0^T dt h(t)h(t). \quad (17)$$

where  $T$  is the observation time.

For a network of independent detectors, the total SNR of a binary are given by:

$$\rho_{\text{total}}^2 = \sum_a \rho_a^2 = \sum_a (h_a|h_a), \quad (18)$$

where the subscript  $a$  stands for quantities related to the  $a$ th detector.

In addition, it is useful to define the characteristic strain  $h_c = A\sqrt{N}$ , with  $N = f_0T$  being the number of binary orbital cycles observed during the mission. Similarly, the noise characteristic strain is defined as

$$h_n(f) = \sqrt{fS_n(f)}, \quad (19)$$

one can straightforwardly estimate SNR from the ratio between  $h_c$  and  $h_n$ .

#### E. Parameter estimation

The uncertainty in the binary parameters can be derived from the FIM  $\Gamma_{ij}$

$$\Gamma_{ij} = \left( \frac{\partial h}{\partial \xi_i} \middle| \frac{\partial h}{\partial \xi_j} \right), \quad (20)$$

where  $\xi_i$  stands for the  $i$ th parameter.

In the high-SNR limit ( $\rho \gg 1$ ), The inverse matrix of the FIM is equal to the covariance matrix,  $\Sigma = \Gamma^{-1}$ . The diagonal elements of the covariance matrix  $\Sigma_{ii}$  give the variance of each parameter  $\Delta\xi_i$ , while the off-diagonal elements represent the covariance.

In numerical calculations, we approximate  $\partial h/\partial\xi_i$  with numerical differentiation:

$$\frac{\partial h}{\partial\xi_i} \approx \frac{\delta h}{\delta\xi_i} \equiv \frac{h(t, \xi_i + \delta\xi_i) - h(t, \xi_i - \delta\xi_i)}{2\delta\xi_i}, \quad (21)$$

where the differentiation steps  $\delta\xi_i$  should be chosen to make the variance  $\Delta\xi_i$  stable [63].

Compared with the uncertainty of each coordinate, we are more interested in sky localization, which is a combination of the uncertainty of both coordinates [64]:

$$\Delta\Omega_S = 2\pi |\sin\beta| \left( \Sigma_{\beta\beta} \Sigma_{\lambda\lambda} - \Sigma_{\beta\lambda}^2 \right)^{1/2}. \quad (22)$$

Similarly to SNR, the total  $\Gamma_{ij}$  of a network is given by:

$$\Gamma_{\text{total}} = \sum_a \Gamma_a = \sum_a \left( \frac{\partial h_a}{\partial\xi_i} \middle| \frac{\partial h_a}{\partial\xi_j} \right), \quad (23)$$

where the subscript  $a$  stands for quantities related to the  $a$ th detector.

#### IV. RESULT

This section presents the results of our analysis of the four detectors mentioned earlier. We begin by evaluating the performance of each detector in standalone operation. We then explore the potential enhancement from operating multiple detectors simultaneously in a network configuration, such as TianQin + LISA, since coordinated observations can significantly improve GW detection capabilities. It should be noted that the designs and orbital configurations of these four detectors differ slightly, and their operation times also vary. Specifically, TianQin has a mission lifetime of 5 years with a duty cycle of 50% [56], while LISA and Taiji share a mission lifetime of 4 years and a duty cycle of 75% [61, 65]. For DECIGO, we adopt the same mission lifetime and duty cycle as LISA and Taiji. All relevant parameters for the four detectors are summarized in Table I.

In this work, we investigate several network configurations ranging from two to four detectors. Hereafter, the following notation is used: TL for TianQin + LISA, TD for TianQin + DECIGO, LD for LISA + DECIGO, TLD for TianQin + LISA + DECIGO, and TLTD for TianQin + LISA + Taiji + DECIGO. In this study, binaries with SNR  $\rho \geq 5$  are treated as VBs. We examine the response of various detector configurations to the candidates VB introduced in Section II, and further assess the uncertainties in parameter estimation for sources with  $\rho \geq 20$ .

#### A. The SNR of verification binaries

We consider 73 sources, calculating the amplitude of these sources listed in Table III. The dimensionless characteristic strain of the binaries is shown in Figure 2 with the sensitivity curves. As shown in Figure 2, the sources are distributed throughout the millihertz band, with DWDs constituting the dominant population. The characteristic strain primarily distributed between the orders of magnitude  $10^{-20}$  and  $10^{-19}$ , with the maximum characteristic strain capable of reaching the magnitude of  $10^{-18}$ . While most sources reside above the DECIGO sensitivity curve (blue dotted line) and only 1 may lie below it, a significant portion fall below the curves of TianQin, LISA, and Taiji, especially for binaries with weak strain amplitudes. This pattern indicates that DECIGO may offer the best individual detection performance, whereas the other three detectors have a more limited reach for the faintest sources.

In Table IV, we report SNRs for all 73 sources under each of the nine considered detector configurations (namely, TianQin, LISA, Taiji, DECIGO, TL, TD, LD, TLD and TLTD), with settings  $\phi_0 = \pi$  and  $\psi_s = \pi/2$ . Consistent with the sensitivity curves, DECIGO achieves the highest SNRs. For instance, sources like CP Eri, V406 Hya, and SDSS J0926 yield an SNR less than 1 with TianQin, but more than 5 with DECIGO. This means that DECIGO has the ability to detect more VBs that cannot be found by TianQin. The SNRs are obviously improved considering the network, as the SNR of the network is given by the root sum squared of the SNRs of the individual detectors [see Eq. (18)]. For example, the SDSS J1908 source yields an SNR of  $\sim 9.2$  with TianQin but reaches  $\sim 82.7$  with TLTD.

The overall detection efficiency across the source catalogue is quantified by counting sources above a range of SNR thresholds. DECIGO alone can detect 71 of the 73 sources, or 97.2% of the total, at a threshold of  $\rho \geq 5$ , substantially outperforming TianQin with 27 sources at 36.9%, LISA with 42 sources at 57.5%, and Taiji with 32 sources at 43.8%. The advantage of DECIGO persists even at higher SNR thresholds: at  $\rho \geq 10$ , it detects 55 sources. Moreover, DECIGO remains the only single detector capable of identifying a significant number of high-SNR systems, detecting 18 sources or 24.7% of the total at  $\rho \geq 100$ . Multi-detector networks significantly enhance these statistics. The complete TLTD configuration detects 58 sources, corresponding to 79.5%, at  $\rho \geq 10$ . Even at the stringent threshold of  $\rho \geq 100$ , networks that include DECIGO consistently identify 18 sources, representing 24.7% of the catalogue. These counts quantitatively confirm that network operations increase the detectability of marginal sources and also expand the sample of high-confidence detections available for precision studies.

The distribution of extreme SNR values across different detector configurations further illustrates the performance differences outlined earlier. Among the single-

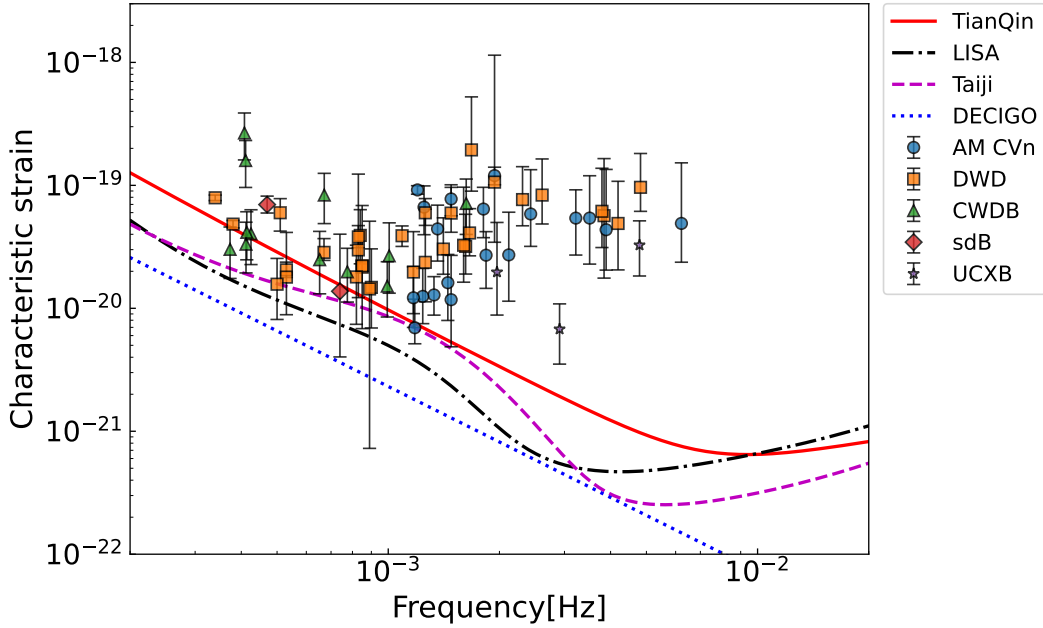


FIG. 2. The characteristic strain versus sensitivity curve. The red solid line, black dash-dot line, magenta dashed line, and blue dotted line correspond to the sensitivity curve of TianQin, LISA, Taiji and DECIGO, respectively, defined in Eqs. (10)-(14). The blue circle, orange square, green triangle, red diamond and purple star represent AM CVn, DWD, CWDB, sdB and UCXB, respectively.

detector setups, TianQin yields SNRs from 0.280 for source SDSS J1436 to 116.137 for source J0806. Notably, LISA and Taiji exhibit a complementary pattern: LISA provides a higher minimum SNR of 1.252 from SDSS J1436 but a lower maximum of 122.114 from ZTF J1539, compared to Taiji's range of 0.777 from SDSS J0926 to 239.567 from J0806. This is a direct consequence of their complementary frequency-dependent sensitivities. LISA is more sensitive at lower frequencies, while Taiji performs better at higher frequencies. DECIGO, by contrast, covers a significantly broader dynamic range, from 4.797 for SDSS J1056 to 803.653 for J0806. In the complete TLTD configuration, the weakest source, SDSS J1056, reaches an SNR of 5.186, while the strongest source, J0806, reaches 854.971.

This performance hierarchy is further quantified by the central tendencies. The mean and median SNRs are 9.8648 and 2.285 for TianQin, 25.9459 and 5.919 for LISA, 25.6036 and 3.838 for Taiji, and 84.4426 and 21.897 for DECIGO. In particular, DECIGO demonstrates superior and more uniform sensitivity, achieving not only the highest maximum and a notably elevated minimum SNR, but also the highest mean and median values, surpassing all other single detectors. The synergy of the complete TLTD network further enhances these capabilities. The overall performance of the network, reflected in a mean SNR of 93.4995 and a median of 23.189, surpasses that of even the best single detector, DECIGO, conclusively underscoring the benefit of multi-detector observations.

In figure 3, we also show the distribution of the num-

ber of sources with SNR greater than 5 in all configurations, taking into account the uncertainty of parameters: pessimistic (Min) and optimistic (Max) estimates correspond to the least and most favorable combinations of parameters, for example, maximum distance and minimum mass versus minimum distance and maximum mass, while the most likely estimate (Med) uses the median value of the parameters. As anticipated, the curves shift systematically towards higher SNR values from the Min to the Med to the Max scenario. The overall distributions are concentrated at lower SNR values with an extended tail toward higher values, indicating that most systems achieve relatively low SNR, with only a minority reaching high SNR levels. A direct comparison of the curve heights across configurations reveals a clear hierarchy in the number of detectable sources. Among single-detector configurations, DECIGO, owing to its superior sensitivity in the millihertz band, shows both a higher total count and a distribution curve that extends further toward higher SNR values, outperforming TianQin, LISA, and Taiji across most of the SNR range. The introduction of multi-detector networks leads to a systematic upward shift of the curves across the entire SNR range, with the distributions also extending further to the right. The complete TLTD network, in particular, results in the most substantial gain, significantly elevating the curve in the high-SNR region. This statistically confirms that coordinated multi-detector observations not only improve the overall SNR of signals but, more importantly, transform a population of systems that would lie near the de-

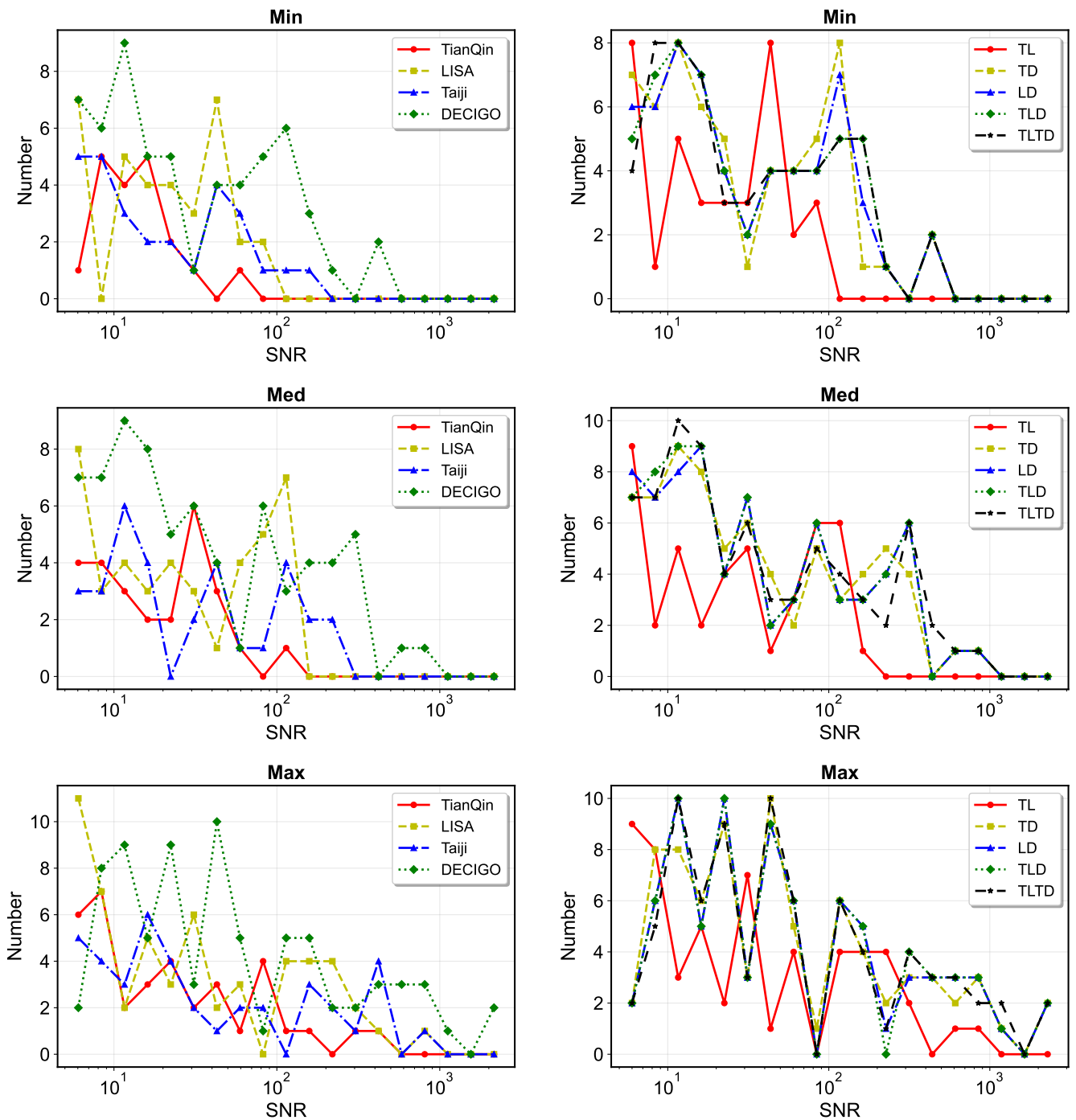


FIG. 3. The left column shows the results for single detectors (TianQin, LISA, Taiji, DECIGO), while the right column shows the results for multi-detector networks (TL, TD, LD, TLD, TLTD). For each configuration, the distributions of pessimistic (Min), most likely (Med), and optimistic (Max) estimates of the SNR are provided.

tection threshold in single-instrument mode into reliably detectable sources. Consequently, such networks effectively expand both the size and depth of the detectable sample, laying an observational foundation for a systematic GW census of Galactic compact binary populations.

In addition, We calculated the SNRs of all sources as

the operational time of different detectors varied from 1 to 5 years. Treating sources with  $\rho \geq 5$  as detectable sources, we calculated the variation over operational time in the number of detectable sources under different detectors. This result is shown in Figure 4. The plot clearly reveals the substantial advantage of multi-detector net-

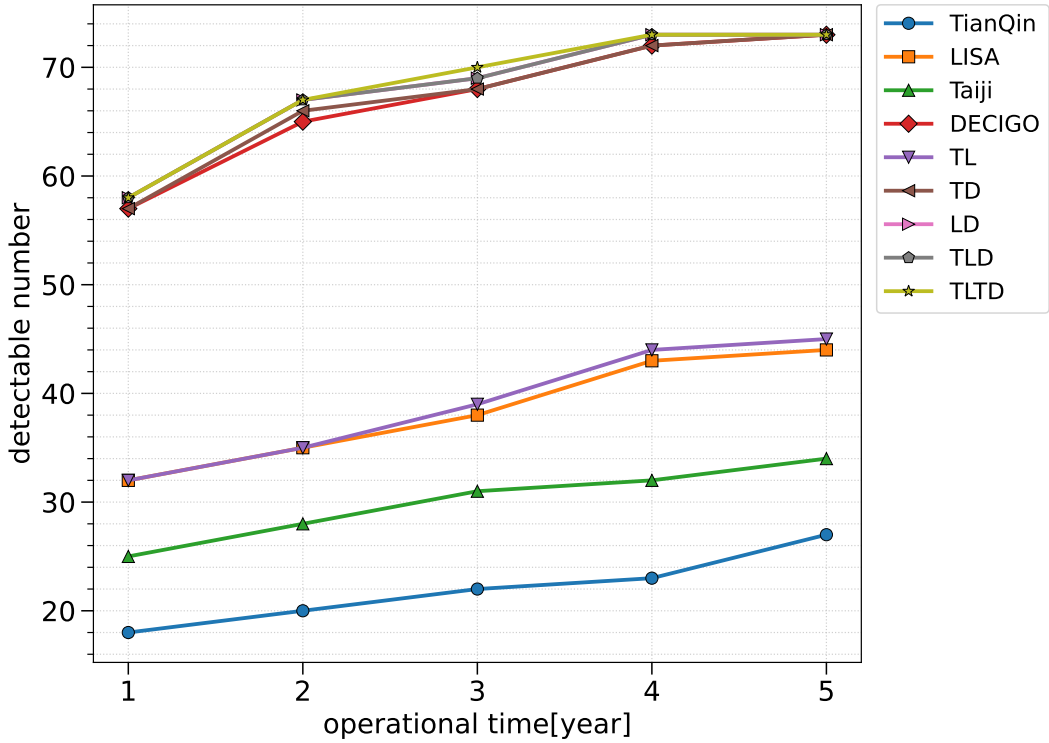


FIG. 4. The detectable number ( $\rho \geq 5$ ) of the 73 VBs over time. Detectors are distinguished by both line colors and marker shapes: TianQin (blue circle), LISA (orange square), Taiji (green triangle up), DECIGO (red diamond), TL (purple triangle down), TD (brown triangle left), LD (pink triangle right), TLD (gray pentagon), and TLTD (olive star).

works and the critical role of long-duration observations. Among single-detector configurations, DECIGO exhibits the fastest growth rate, requiring only about 1 year of observation to surpass the final 5-year detection count of other single instruments. This capability stems from its exceptional sensitivity in the millihertz range and the mode in which multiple satellites operate simultaneously (see Table I). TianQin shows a relatively flatter growth curve. This is influenced by its specific mission profile, which includes a 50% duty cycle, while LISA and Taiji follow similar growth trajectories. The synergistic effect of multi-detector networks is particularly striking: the TLTD network curve remains at the top throughout, culminating in a final detectable source count that far exceeds that of any single detector. This demonstrates that networks not only enhance the SNR of individual sources through combined data but also systematically increase the total number of resolvable sources on a population level. This result strongly supports the scientific necessity of future coordinated multi-mission observations and maximizing mission lifetimes, which is essential for constructing a more complete census of Galactic compact binary GW sources.

## B. the parameter estimation of verification binaries

To assess the scientific potential of GW observations, we performed a detailed parameter estimation for VBs with  $\rho \geq 20$  in various network configurations. Using the FIM formalism described in Section III E, we quantified the measurement precision for key binary parameters including chirp mass ( $\mathcal{M}_c$ ), distance ( $d$ ), inclination angle ( $\iota$ ) and sky localization ( $\Omega$ ). Table V illustrates the relative uncertainties for the 40 VBs under different detector configurations.

As a single detector, DECIGO consistently delivers the highest parameter estimation precision due to its superior sensitivity in the millihertz band. For high-SNR systems such as J0806 and ZTF J1539, DECIGO measures chirp masses with exquisite relative uncertainties below 0.2%, constrains distances to within about 10%, determines inclination angles  $\iota$  to better than approximately 1%, and achieves precise sky localization at the level of  $\Delta\Omega_S \sim 10^{-6} - 10^{-4} \text{ deg}^2$ . Nevertheless, it is noteworthy that although DECIGO provides the deepest reach, the average relative uncertainties across its entire catalogue are higher than those of other single detectors, with  $\langle \sigma_{\mathcal{M}_c} / \mathcal{M}_c \rangle \sim 14.24$  and  $\langle \sigma_d / d \rangle \sim 23.76$ . This reflects its unique ability to probe fainter and more distant systems, which are inherently more difficult to characterize, thereby expanding the observable parameter space at the

cost of larger average uncertainties for the faintest detections.

Multi-detector configurations significantly improve parameter estimation accuracy. For exceptionally high-SNR systems such as J0806, the TLTD network achieves extraordinary precision: chirp mass relative uncertainty can drop below 0.01%, distance estimates are constrained to about 1%, inclination angles to better than 5%, and sky localization is refined to the level of  $10^{-5} \text{ deg}^2$ . More importantly, this enhanced precision is not limited to a few outstanding sources but extends robustly across the entire detectable population. For the catalogue of 40 sources, the network yields dramatically reduced median uncertainties:  $4.99 \times 10^{-4} \text{ deg}^2$  for sky location,  $1.55 \times 10^{-2} M_{\odot}$  for chirp mass, 0.128 kpc for distance, and  $0.781^{\circ}$  for inclination.

The chirp mass, which directly determines the GW amplitude, can be constrained with high precision for the majority of detectable sources. Among single detectors, Taiji achieves the tightest median constraint of  $\sigma_{\mathcal{M}_c} = 1.37 \times 10^{-2} M_{\odot}$  for its 16 sources with  $\rho \geq 20$ , followed by TianQin with  $4.64 \times 10^{-2} M_{\odot}$  for 12 sources, and LISA with  $8.91 \times 10^{-2} M_{\odot}$  for 24 sources. DECIGO, while detecting the largest sample of 39 sources, exhibits a significantly larger median uncertainty of  $1.75 \times 10^{-1} M_{\odot}$  and the highest average relative uncertainty of  $\langle \sigma_{\mathcal{M}_c} / \mathcal{M}_c \rangle \sim 14.24$ , which reflects its unique sensitivity to a fainter and more challenging population of distant systems. Network configurations dramatically improve and homogenize the measurement precision. The complete TLTD network delivers a median  $\sigma_{\mathcal{M}_c}$  of  $1.55 \times 10^{-2} M_{\odot}$  across 40 sources — a precision comparable to the best single detector, Taiji, but for a sample nearly three times as large. Furthermore, the average relative uncertainty of network drops to approximately 1.188, representing an order-of-magnitude improvement over DECIGO and clearly demonstrating the power of multi-detector networks to break parameter degeneracies.

Precise distance measurement is critical for determining the spatial positions of GW sources. The performance of individual detectors varies significantly: Taiji again delivers the best median precision with  $\sigma_d = 0.17 \text{ kpc}$ , while DECIGO exhibits a larger median uncertainty of 1.325 kpc and the highest average relative uncertainty, measured as  $\langle \sigma_d / d \rangle \sim 23.76$ . The synergy achieved in multi-detector networks substantially compresses these distance uncertainties. For the complete TLTD network, the median  $\sigma_d$  improves to 0.128 kpc, and the average relative uncertainty decreases to approximately 1.99. This uniform improvement across the entire catalogue, highlights the unique capability of network for distance determination.

The inclination angle, key to breaking the distance-inclination degeneracy, presents the widest range of uncertainties. Single detectors show significant scatter: Taiji and TianQin offer median precisions of  $0.834^{\circ}$  and  $2.074^{\circ}$ , respectively. In stark contrast, the median uncertainty of DECIGO is  $12.258^{\circ}$ , with extreme outliers that

max  $\sigma_i > 100^{\circ}$ , indicating sources with virtually unconstrained inclination. Networks provide a revolutionary improvement. Even a two-detector network like TD reduces the median  $\sigma_i$  to  $0.952^{\circ}$ . The complete TLTD network achieves a median of  $0.781^{\circ}$  and confines the maximum uncertainty to  $\sim 60^{\circ}$ , effectively enabling reliable inclination determination for the entire high-SNR population, which is essential for astrophysical interpretation.

Sky localization accuracy reflects the detector's ability to spatially locate a source. Here, the advantage of networks is most dramatic. While DECIGO achieves an excellent single detector median of  $5.2 \times 10^{-3} \text{ deg}^2$ , other single detectors have median values larger by 1-2 orders of magnitude (e.g., LISA:  $8.78 \times 10^{-2} \text{ deg}^2$ ). Networks, by synthesizing information from spatially separated detectors, improve localization by multiple orders of magnitude. The progression is clear: the TL network reaches a median of  $6.92 \times 10^{-3} \text{ deg}^2$ , the TLD network improves to  $5.19 \times 10^{-4} \text{ deg}^2$ , and the complete TLTD network delivers the ultimate precision of  $4.99 \times 10^{-4} \text{ deg}^2$ . This corresponds to localizing sources to areas on the sky thousands of times smaller than those achievable by most single detectors.

## V. CONCLUSION

This study presents a systematic framework for evaluating the detectability and parameter estimation of Galactic binaries with the space-based GW detectors TianQin, LISA, Taiji, and DECIGO. Moving beyond individual mission capabilities, we quantify the enhanced potential of a coordinated multi-detector network. Our analysis is grounded in a catalogue of known candidate *verification binaries* (CVBs) identified through EM observations, and employs a combination of analytical expressions and numerical methods to compute instrument noise curves, SNRs and parameter estimation uncertainties.

Among the 73 VBs detectable by the TLTD network, individual detectors exhibit varying coverage: TianQin can detect 27, LISA 42, Taiji 32, and DECIGO 71 of these systems. The highest-SNR source for TianQin, Taiji, and DECIGO is J0806, while for LISA it is ZTF J1539. Notably, DECIGO alone achieves the greatest single-detector SNR for J0806, exceeding 800. In all network configurations considered, J0806 remains the strongest source, with the complete TLTD network delivering the highest combined SNR of over 850. This not only underscores the exceptional suitability of J0806 as a VB, but also highlights the superior sensitivity of DECIGO to high-SNR sources compared to other single detectors—an advantage that is further amplified in multi-detector networks. Beyond the brightest sources, DECIGO yields higher SNRs than any other single detector across the entire catalogue, demonstrating its outstanding depth and breadth of detection, a capability that is enhanced even further in the combined TLTD configuration.

The distribution of detectable sources as a function of SNR further elucidates the performance hierarchy. Among single detectors, DECIGO not only yields the highest number of detections but also shifts the SNR distribution markedly toward higher values, confirming its superior sensitivity within the millihertz band. The integration of detectors into networks, particularly the complete TLTD configuration, systematically increases the number of sources across all SNR bins. Most notably, it transforms a substantial population of systems that would reside near the detection threshold for any single instrument into confidently detectable sources, thereby expanding the observable sample both in size and depth.

The number of detectable sources exhibits a strong dependence on the operational time. While all configurations show growth over time, DECIGO achieves the most rapid gain, surpassing the final 5-year detection count of other single detectors within approximately one year of observation. This rapid convergence underscores its exceptional design sensitivity. Multi-detector networks, however, unlock the most significant gains in survey efficiency. The TLTD network consistently provides the highest yield at any given mission time, culminating in a final count that far exceeds that of any standalone instrument. This result underscores the critical importance of long, coordinated missions for compiling a complete census of Galactic GW sources.

FIM analysis reveals that key binary parameters—including chirp mass, distance, inclination, and sky location—can be constrained with remarkable precision for high-SNR systems within a network. While single detectors like Taiji provide excellent parameter estimation for the brightest sources, network configurations dramatically reduce uncertainties across the entire de-

tectable population. The TLTD network, in particular, achieves median precisions of  $\sim 1.6 \times 10^{-2} M_{\odot}$  in chirp mass,  $\sim 0.13$  kpc in distance,  $\sim 0.82^{\circ}$  in inclination, and  $\sim 6.1 \times 10^{-4} \text{ deg}^2$  in sky localization. This order-of-magnitude improvement in sky localization is pivotal, as it enables the unambiguous identification of EM counterparts and facilitates detailed multi-messenger astrophysics.

We are entering an era of multi-messenger synergy included EM and GW surveys. We show that space-based GW detectors, especially when operated as a coordinated network, have the potential to complement these surveys by delivering precise dynamical parameters for thousands of systems. This combined approach will enable population-level studies, constrain binary evolution models, and deepen our understanding of compact object physics across the Milky Way.

## VI. ACKNOWLEDGMENTS

The work has been supported by the CPSF Postdoctoral Fellowship Program (Grant No. GZC20242112); Guangdong Provincial Key Laboratory of Advanced Particle Detection Technology (2024B1212010005); Guangdong Provincial Key Laboratory of Gamma-Gamma Collider and Its Comprehensive Applications (2024KSYS001); National Key Program for S&T Research and Development (2023YFA1607200).

### Appendix A: table of verification binaries

TABLE III: The Sample of Candidate Verification Binaries. Notes: 1. Square brackets represent the estimated values. 2. The distance parameter is derived from the parallax provided by Gaia DR3. 3. The right column uses Roman numerals to denote the sources from which the parameters of these sources are taken: (i) Ref. [38], (ii) Ref. [66], (iii) Ref. [67], (iv) Ref. [68], (v) Ref. [51], (vi) Ref. [28], (vii) Ref. [69], (viii) Ref. [70], (ix) Ref. [71], (x) Ref. [72], (xi) Ref. [73], (xii) Ref. [74], (xiii) Ref. [75], (xiv) Ref. [76], (xv) Ref. [77], (xvi) Ref. [78], (xvii) Ref. [79], (xviii) Ref. [80], (xix) Ref. [81], (xx) Ref. [82], (xxi) Ref. [83], (xxii) Ref. [84], (xxiii) Ref. [85], (xxiv) Ref. [86], (xxv) Ref. [87], (xxvi) Ref. [88], (xxvii) Ref. [44], (xxviii) Ref. [54], (xxix) Ref. [89], (xxx) Ref. [90], (xxxi) Ref. [91], and the references therein.

Source	$\lambda$ [deg]	$\beta$ [deg]	$f$ [mHz]	$d$ [kpc]	$M$ [ $M_{\odot}$ ]	$m$ [ $M_{\odot}$ ]	$\iota$ [deg]	Refs.
<b>AM CVn</b>								
J0806	120.4425	-4.704	6.22	[5.0 $\pm$ 3.0]	0.55 $\pm$ 0.05	0.27 $\pm$ 0.05	38	i,ii
ATLAS J1013	179.4384	-51.0003	3.89	1.802 $\pm$ 0.639	0.87 <sup>+0.36</sup> <sub>-0.25</sub>	0.10 <sup>+0.03</sup> <sub>-0.02</sub>	[82]	iii
V407 Vul	294.9945	46.7829	3.51	2.087 $\pm$ 0.676	[0.8 $\pm$ 0.1]	[0.177 $\pm$ 0.071]	[60]	i
ES Cet	24.612	-20.3339	3.22	1.727 $\pm$ 0.21	[0.8 $\pm$ 0.1]	[0.161 $\pm$ 0.064]	[60]	i
ZTF J0127	43.1707	40.009	2.43	1.283 $\pm$ 0.604	0.75 $\pm$ 0.06	0.19 $\pm$ 0.03	[80]	iv

*Continued on next page*

TABLE III – *Continued from previous page*

Source	$\lambda$ [deg]	$\beta$ [deg]	$f$ [mHz]	$d$ [kpc]	$M$ [ $M_{\odot}$ ]	$m$ [ $M_{\odot}$ ]	$i$ [deg]	Refs.
SDSS J1351	208.3879	4.4721	2.12	$1.341 \pm 0.436$	$[0.8 \pm 0.1]$	$[0.1 \pm 0.040]$	[60]	i
AM CVn	170.3858	37.4427	1.94	$0.302 \pm 0.003$	$0.68 \pm 0.06$	$0.125 \pm 0.012$	43	i
SDSS J1908	298.2172	61.4542	1.84	$0.977 \pm 0.032$	$[0.8 \pm 0.1]$	$[0.085 \pm 0.034]$	15	i
HP Lib	235.0882	4.9597	1.81	$0.28 \pm 0.002$	$0.645 \pm 0.155$	$0.068 \pm 0.02$	30	i
TIC378898110	215.5392	-52.6045	1.48	$0.309 \pm 0.002$	$[0.6 \pm 0.1]$	$0.1^{+0.02}_{-0.02}$	$74 \pm 10.0$	v
PTF1 J1919	309.0023	69.029	1.48	$1.365 \pm 0.474$	$[0.8 \pm 0.1]$	$[0.066 \pm 0.026]$	[60]	i
CXOGBS J1751	268.0614	-6.2526	1.45	$0.939 \pm 0.102$	$[0.8 \pm 0.1]$	$[0.064 \pm 0.026]$	[60]	i
CR Boo	202.2728	17.8971	1.36	$0.352 \pm 0.005$	$0.885 \pm 0.215$	$0.066 \pm 0.022$	30	i
KL Dra	334.1334	78.3217	1.33	$0.922 \pm 0.088$	$0.76 \pm 0.1$	$0.057 \pm 0.01$	[60]	vi,vii
V803 Cen	216.1673	-30.3166	1.25	$0.287 \pm 0.005$	$0.975 \pm 0.195$	$0.084 \pm 0.025$	13.5	i
PTF1 J0719	104.3883	26.5213	1.24	$0.841 \pm 0.201$	$[0.8 \pm 0.1]$	$[0.053 \pm 0.01]$	[60]	viii
SMSS J1138	202.6662	-47.997	1.2	$0.547 \pm 0.018$	$0.99^{+0.01}_{-0.01}$	$0.24^{+0.01}_{-0.01}$	$88.7 \pm 0.1$	ix
SDSS J0926	132.2867	20.2342	1.18	$0.814 \pm 0.165$	$0.84 \pm 0.05$	$0.029^{+0.009}_{-0.002}$	82.6	x
CP Eri	42.1327	-26.4276	1.17	$0.748 \pm 0.203$	$[0.8 \pm 0.1]$	$[0.049 \pm 0.01]$	[60]	i,viii
V406 Hya	140.7336	-21.2342	0.99	$0.736 \pm 0.231$	$[0.8 \pm 0.1]$	$[0.04 \pm 0.01]$	[60]	i,viii
<b>DWD</b>								
ZTF J1539	205.0315	66.1616	4.82	$1.629 \pm 0.693$	$0.61^{+0.017}_{-0.022}$	$0.21^{+0.014}_{-0.015}$	84	xi
ZTF J0546	87.2578	15.3132	4.19	$3.707^{+1.631}_{-1.258}$	$[0.6 \pm 0.1]$	$[0.3 \pm 0.1]$	[60]	xii
ZTF J1858	283.1123	2.3905	3.84	$2.895^{+2.733}_{-1.449}$	$[0.6 \pm 0.1]$	$[0.3 \pm 0.1]$	[60]	xii
ZTF J2243	13.2423	53.9599	3.79	$1.753 \pm 0.72$	$0.323 \pm 0.065$	$0.335 \pm 0.054$	$82.1 \pm 0.5$	xiii
SDSS J0651	101.3396	5.8048	2.61	$0.958 \pm 0.371$	$0.50 \pm 0.04$	$0.26 \pm 0.04$	86.9	i
ZTF J0538	84.8061	-3.4356	2.31	$0.997 \pm 0.364$	$0.45 \pm 0.05$	$0.32 \pm 0.03$	$85.4 \pm 0.1$	xiv
ZTF J1905	293.7825	53.6335	1.94	$0.696 \pm 0.602$	$[0.6 \pm 0.1]$	$[0.3 \pm 0.1]$	[60]	xiv
SDSS J0935	130.9795	28.0912	1.68	$0.396 \pm 0.205$	$0.312 \pm 0.019$	$0.75 \pm 0.24$	[60]	i
SDSS J2322	353.4373	8.4572	1.66	$0.86 \pm 0.204$	$0.31 \pm 0.02$	$0.29 \pm 0.05$	27	xv
PTF J0533	82.9097	-21.1234	1.62	$1.172 \pm 0.389$	$0.652 \pm 0.04$	$0.167 \pm 0.03$	72.8	xvi
ZTF J2029	314.4631	33.4205	1.6	$1.095 \pm 0.643$	$0.32 \pm 0.04$	$0.3 \pm 0.04$	$86.6 \pm 0.1$	xvii
J1239	197.4157	-15.0625	1.48	$0.972 \pm 0.272$	$0.291 \pm 0.013$	$0.68^{+0.11}_{-0.06}$	$71^{+8.0}_{-10.0}$	v, xviii
ZTF J0722	115.8782	-40.2164	1.41	$1.267 \pm 0.442$	$0.38 \pm 0.04$	$0.33 \pm 0.03$	$89.7 \pm 0.2$	xvii
ZTF J1749	267.0209	32.8576	1.26	$1.291 \pm 0.665$	$0.4 \pm 0.07$	$0.28 \pm 0.05$	$85.5 \pm 1.4$	xiv
SDSS J0634	97.0832	14.839	1.26	$0.435^{+0.016}_{-0.015}$	$0.45^{+0.07}_{-0.06}$	$0.21^{+0.03}_{-0.02}$	$43^{+7.0}_{-5.6}$	xix
ZTF J2228	7.0683	53.2065	1.17	$2.076 \pm 0.657$	$[0.6 \pm 0.1]$	$[0.3 \pm 0.1]$	[60]	xiv
SMSS J0338	286.4357	-72.7068	1.09	$0.536 \pm 0.016$	$0.23 \pm 0.015$	$0.38 \pm 0.05$	$69 \pm 9.0$	xx
ZTF J0643	101.5702	-19.6948	0.9	$2.04 \pm 0.597$	$[0.6 \pm 0.1]$	$[0.3 \pm 0.1]$	[60]	xxi
ZTF J0640	99.6432	-5.4567	0.89	$1.576 \pm 0.62$	$0.39 \pm 0.12$	$0.325 \pm 0.3$	$65.3 \pm 5.1$	xiv
SDSS J0106	11.4582	-15.7928	0.85	$0.825 \pm 0.438$	$0.188 \pm 0.1$	$0.57 \pm 0.01$	67	i,vi
ZTF J2130	348.1685	54.4443	0.85	$1.307 \pm 0.043$	$0.545 \pm 0.02$	$0.337 \pm 0.015$	$86.4 \pm 1.0$	xxii
SDSS J1630	231.7612	63.0501	0.84	$0.848 \pm 0.167$	$0.298 \pm 0.019$	$0.76 \pm 0.24$	[60]	i
SDSS J0822	120.6816	11.0965	0.83	$0.837 \pm 0.574$	$0.304 \pm 0.1$	$0.524 \pm 0.01$	88.1	i,vi
J1526	235.9907	-8.1906	0.83	$0.625 \pm 0.075$	$0.37 \pm 0.02$	$0.4 \pm 0.02$	[60]	xxiii
ZTF J1901	306.8131	74.6335	0.82	$0.909 \pm 0.078$	$0.5 \pm 0.1$	$0.2 \pm 0.1$	86.2	xxiv
SDSS J1235	181.7907	17.9525	0.67	$0.446 \pm 0.028$	$0.35 \pm 0.01$	$0.27^{+0.06}_{-0.02}$	$27 \pm 3.8$	v
SDSS J0056	10.6273	-11.3044	0.53	$0.627 \pm 0.046$	$0.18 \pm 0.01$	$0.82 \pm 0.02$	[60]	i,vi
SDSS J1056	130.4076	52.2268	0.53	$1.198 \pm 0.536$	$0.334 \pm 0.1$	$0.76 \pm 0.01$	[60]	i,vi
SDSS J0923	133.7151	14.4268	0.51	$0.288 \pm 0.005$	$0.275 \pm 0.015$	$0.76 \pm 0.23$	[60]	i
SDSS J1436	187.5011	59.9313	0.5	$0.943 \pm 0.13$	$0.234 \pm 0.1$	$0.78 \pm 0.01$	[60]	i,vi
WD 0957	208.5263	-67.3013	0.38	$0.164 \pm 0.001$	$0.37 \pm 0.013$	$0.32 \pm 0.013$	68	i,vi
SDSS J1337	182.8931	45.5716	0.34	$0.114 \pm 0.001$	$0.51 \pm 0.01$	$0.32 \pm 0.01$	$34 \pm 1.0$	xxv
WD 1242	194.5586	-5.552	0.19	$0.04 \pm 0.0$	$0.56^{+0.05}_{-0.07}$	$0.39^{+0.04}_{-0.05}$	45.1	i,vi
WD 1704	242.3234	70.1865	0.16	$0.039 \pm 0.0$	$0.39 \pm 0.05$	$0.56 \pm 0.07$	[60]	xxvi
<b>CWDB</b>								
ZTF J0526	84.6989	36.2955	1.63	$0.845 \pm 0.067$	$[0.6 \pm 0.1]$	$[0.3 \pm 0.1]$	[60]	xxvii
ZTF J1840	279.7729	5.3797	1.01	$1.286 \pm 0.277$	$[0.6 \pm 0.1]$	$[0.3 \pm 0.1]$	[60]	xxvii
ZTF J1707	257.2883	7.4854	0.99	$2.236 \pm 0.176$	$[0.6 \pm 0.1]$	$[0.3 \pm 0.1]$	[60]	xxvii
ZTF J2351	36.8445	55.5895	0.78	$1.28 \pm 0.081$	$[0.6 \pm 0.1]$	$[0.3 \pm 0.1]$	[60]	xxvii
ZTF J1611	183.9170	78.0916	0.67	$0.257 \pm 0.008$	$[0.6 \pm 0.1]$	$[0.3 \pm 0.1]$	[60]	xxvii
ZTF J1813	276.0031	66.2346	0.65	$0.834 \pm 0.12$	$[0.6 \pm 0.1]$	$[0.3 \pm 0.1]$	[60]	xxvii
ZTF J1603	232.8645	41.6031	0.43	$0.312 \pm 0.023$	$[0.6 \pm 0.1]$	$[0.3 \pm 0.1]$	[60]	xxvii
ZTF J0451	71.5210	-21.2702	0.41	$0.294 \pm 0.003$	$[0.6 \pm 0.1]$	$[0.3 \pm 0.1]$	[60]	xxvii

*Continued on next page*

TABLE III – *Continued from previous page*

Source	$\lambda$ [deg]	$\beta$ [deg]	$f$ [mHz]	$d$ [kpc]	$M$ [ $M_{\odot}$ ]	$m$ [ $M_{\odot}$ ]	$i$ [deg]	Refs.
ZTF J0112	44.5245	45.8154	0.41	$0.365 \pm 0.013$	$[0.6 \pm 0.1]$	$[0.3 \pm 0.1]$	[60]	xxvii
ZTF J2334	12.6230	38.0721	0.41	$0.076 \pm 0.0$	$[0.6 \pm 0.1]$	$[0.3 \pm 0.1]$	[60]	xxvii
ZTF J2007	309.0298	36.9204	0.41	$0.045 \pm 0.0$	$[0.6 \pm 0.1]$	$[0.3 \pm 0.1]$	[60]	xxvii
ZTF J1943	293.0642	-5.5741	0.37	$0.358 \pm 0.015$	$[0.6 \pm 0.1]$	$[0.3 \pm 0.1]$	[60]	xxvii
ZTF J1708	258.3723	-2.8898	0.37	$0.109 \pm 0.001$	$[0.6 \pm 0.1]$	$[0.3 \pm 0.1]$	[60]	xxvii
<b>sdB</b>								
OW J0741	125.3546	-50.1862	0.74	$1.576 \pm 0.644$	$0.23 \pm 0.12$	$0.72 \pm 0.17$	57.4	xxviii
CD-30	221.1718	-16.6125	0.47	$0.355 \pm 0.006$	$0.47_{-0.06}^{+0.07}$	$0.74 \pm 0.02$	82.9	xxix
HD 265435	101.3387	10.1442	0.34	$0.461 \pm 0.012$	$0.63_{-0.12}^{+0.13}$	$1.01 \pm 0.15$	$64_{-5.0}^{+14.0}$	v
<b>UCXB</b>								
1RXS J1718	261.7319	-17.35	4.79	$6.5 \pm 0.5$	$[0.6 \pm 0.1]$	$[0.3 \pm 0.1]$	[60]	xxx
4U 1820-30	275.1436	-7.0275	2.91	$7.972 \pm 0.277$	$[1.4 \pm 0.6]$	$[0.069 \pm 0.015]$	[60]	v
4U 0513-40	70.602	-62.7122	1.97	$6.466_{-3.134}^{+4.941}$	$[0.6 \pm 0.1]$	$[0.55 \pm 0.1]$	[60]	xxxi

**Appendix B: snr of verification binaries**

The SNR of all selected binaries are listed in Table IV, assuming a nominal mission lifetime of five years for

TianQin and four years for LISA, Taiji, and DECIGO, with settings  $\phi_0 = \pi$  and  $\psi_S = \pi/2$  for all binaries.

TABLE IV: The SNR of VBs with single detector and the network of them.  $\mathcal{A}$  is given in units in  $10^{-23}$ .

Source	$\mathcal{A}$	SNR								
		TQ	LISA	Taiji	DECIGO	TL	TD	LD	TLTLD	TLTD
<b>AM CVn</b>										
J0806	6.39	116.137	119.129	239.567	803.653	166.512	812.03	811.118	820.722	854.971
ATLAS J1013	7.18	26.296	54.542	80.007	160.090	59.725	161.929	168.503	170.868	188.671
V407 Vul	9.4	35.518	90.452	110.747	238.992	97.147	241.605	253.819	257.982	280.748
ES Cet	9.81	16.294	103.034	104.49	253.276	104.476	253.866	271.626	273.978	293.227
ZTF J0127	12.2	9.652	53.949	29.888	108.036	54.773	108.449	117.885	121.127	124.760
SDSS J1351	6.07	4.372	27.112	12.936	69.004	27.538	69.172	73.401	74.296	75.414
AM CVn	28.01	30.917	107.262	49.506	265.47	111.343	267.146	282.79	287.875	292.101
SDSS J1908	6.48	9.209	31.845	14.683	74.368	33.148	74.935	80.484	81.421	82.735
HP Lib	15.5	16.372	68.753	31.76	162.238	70.599	163.029	173.972	176.933	179.761
TIC378898110	20.72	6.211	23.904	11.848	79.074	24.722	79.325	81.794	82.848	83.691
PTF1 J1919	3.14	1.495	3.888	1.927	16.457	4.119	16.513	16.859	16.964	17.073
CXOGBS J1751	4.36	3.124	5.787	2.895	20.235	6.56	20.47	20.912	21.272	21.468
CR Boo	12.33	5.237	22.211	11.441	85.421	22.903	85.603	87.782	88.438	89.175
KL Dra	3.62	1.149	3.726	1.939	16.724	3.951	16.776	17.066	17.185	17.294
V803 Cen	19.33	7.476	24.908	13.312	117.631	26.309	117.936	119.565	120.537	121.270
PTF1 J0719	3.65	1.887	3.61	1.936	14.74	4.104	14.869	15.092	15.301	15.423
SMSS J1138	27.24	5.07	13.141	7.142	49.31	13.927	49.525	50.646	51.239	51.734
SDSS J0926	2.08	0.686	1.421	0.777	5.73	1.616	5.782	5.851	5.954	6.004
CP Eri	3.66	0.871	2.964	1.627	12.517	3.116	12.553	12.852	12.899	13.001
V406 Hya	2.72	0.968	1.447	0.844	6.808	1.746	6.878	6.947	7.028	7.079
<b>DWD</b>										
ZTF J1539	14.27	39.76	122.114	222.095	597.212	128.94	598.645	608.028	610.973	650.088
ZTF J0546	7.78	42.847	109.425	176.748	326.19	117.755	329.078	341.037	346.794	389.238
ZTF J1858	9.4	52.832	105.151	151.238	315.977	117.514	320.304	330.312	337.122	369.492
ZTF J2243	10.27	20.003	83.834	118.091	254.614	86.593	255.535	265.257	268.936	293.721
SDSS J0651	16.77	27.459	77.06	48.46	180.465	80.945	182.158	193.994	197.788	203.638
ZTF J0538	16.39	18.951	79.177	40.888	162.916	81.636	164.125	178.068	182.226	186.757
ZTF J1905	24.8	26.375	79.443	36.667	224.158	84.077	225.842	236.491	239.407	242.198
SDSS J0935	48.71	46.878	106.352	50.042	288.655	115.893	292.305	303.477	311.051	315.051
SDSS J2322	10.34	11.865	33.291	15.729	90.037	35.279	90.791	95.001	96.702	97.973

*Continued on next page*

TABLE IV – *Continued from previous page*

Source	$\mathcal{A}$	SNR								
		TQ	LISA	Taiji	DECIGO	TL	TD	LD	TLD	TLTD
PTF J0533	8.15	5.317	11.283	5.38	33.968	12.355	34.339	35.521	36.145	36.543
ZTF J2029	8.37	4.761	9.3	4.456	31.9	10.537	32.282	33.097	33.595	33.889
J1239	15.89	5.351	18.372	9.106	62.564	19.089	62.778	64.701	65.411	66.042
ZTF J0722	8.3	3.476	7.858	3.982	27.68	8.792	27.96	28.664	29.043	29.315
ZTF J1749	6.85	2.172	5.957	3.173	19.677	6.438	19.828	20.451	20.703	20.945
SDSS J0634	17.32	12.809	23.001	12.251	90.711	26.373	91.624	93.159	94.467	95.258
ZTF J2228	5.93	1.529	3.746	2.056	18.016	3.978	18.066	18.328	18.45	18.564
SMSS J0338	12.12	2.201	6.702	3.779	31	7.117	31.092	31.545	31.806	32.030
ZTF J0643	5.07	1.505	2.516	1.517	10.087	2.925	10.197	10.369	10.503	10.611
ZTF J0640	4.95	1.32	2.251	1.362	8.749	2.61	8.848	8.992	9.13	9.231
SDSS J0106	7.61	0.908	2.896	1.779	11.585	3.02	11.617	11.892	11.972	12.104
ZTF J2130	7.82	0.857	1.433	0.88	5.877	1.606	5.922	6.016	6.092	6.156
SDSS J1630	13.89	1.709	5.111	3.153	26.25	5.392	26.306	26.696	26.798	26.983
SDSS J0822	10.65	1.761	2.236	1.385	11.595	2.765	11.708	11.765	11.92	12.000
J1526	13.58	1.954	5.287	3.275	21.649	5.613	21.731	22.183	22.365	22.603
ZTF J1901	6.46	0.607	1.919	1.193	8.825	2.065	8.858	9.007	9.064	9.142
SDSS J1235	11.32	1.632	5.315	3.543	14.223	5.53	14.304	15.026	15.26	15.666
SDSS J0056	9.17	0.47	1.642	1.187	4.918	1.694	4.935	5.137	5.201	5.335
SDSS J1056	8.01	0.525	1.534	1.108	4.797	1.628	4.828	4.978	5.066	5.186
SDSS J0923	27.25	2.513	4.387	3.211	14.681	5.016	14.881	15.243	15.514	15.843
SDSS J1436	7.22	0.28	1.252	0.923	5.584	1.296	5.594	5.703	5.733	5.807
WD 0957	25.51	0.498	2.512	2.032	9.205	2.599	9.229	9.471	9.565	9.778
SDSS J1337	44.16	1.184	5.442	4.581	13.779	5.609	13.846	14.661	14.877	15.567
WD 1242	109.24	0.754	3.816	4.207	13.265	3.92	13.295	13.71	13.832	14.458
WD 1704	99.91	0.376	1.418	1.666	7.549	1.501	7.565	7.668	7.697	7.875
<b>CWDB</b>										
ZTF J0526	18.16	12.78	38.183	18.179	111.783	40.35	112.542	116.659	118.843	120.225
ZTF J1840	8.66	3.298	5.919	3.435	21.897	6.814	22.156	22.561	22.933	23.189
ZTF J1707	4.94	1.476	3.274	1.907	12.012	3.606	12.106	12.372	12.541	12.686
ZTF J2351	7.31	0.679	2.513	1.593	9.818	2.589	9.838	10.076	10.154	10.278
ZTF J1611	33.09	2.285	9.474	6.312	41.196	9.963	41.311	42.111	42.384	42.851
ZTF J1813	10	0.902	2.632	1.771	12.327	2.813	12.367	12.586	12.644	12.768
ZTF J1603	20.1	0.665	2.573	2.002	6.469	2.669	6.508	6.906	6.998	7.279
ZTF J0451	20.96	0.923	2.801	2.199	7.216	2.949	7.275	7.709	7.795	8.100
ZTF J0112	16.83	0.433	2.111	1.66	5.276	2.169	5.3	5.601	5.705	5.941
ZTF J2334	80.7	2.371	10.056	7.915	25.083	10.371	25.211	26.664	27.142	28.273
ZTF J2007	135.63	7.199	17.477	13.79	42.196	18.966	42.834	45.331	46.262	48.274
ZTF J1943	16.06	0.815	1.871	1.523	5.091	2.043	5.156	5.375	5.485	5.693
ZTF J1708	52.55	2.044	4.706	3.838	16.908	5.136	17.032	17.434	17.671	18.083
<b>sdB</b>										
OW J0741	5.2	0.858	1.783	1.148	7.153	1.968	7.201	7.357	7.419	7.507
CD-30	33.07	0.909	2.5	1.881	10.348	2.631	10.38	10.58	10.677	10.842
HD 265435	33.93	1.126	2.84	2.391	9.285	3.066	9.356	9.64	9.778	10.066
<b>UCXB</b>										
1RXS J1718	4.85	31.404	61.203	110.873	236.878	68.534	238.877	243.136	246.593	270.372
4U 1820-30	1.29	3.972	12.491	9.971	26.046	13.106	26.347	28.394	29.158	30.816
4U 0513-40	4.56	3.614	13.529	6.261	49.195	14.014	49.331	50.89	51.152	51.534

### Appendix C: parameters estimation of verification binaries

The estimation of parameters for VBs is listed in Table V, including the uncertainty of the four key parameters,

chirp mass, distance, inclination, and sky localization.

TABLE V: Uncertainties on  $M_c$ ,  $d$ ,  $\iota$  and  $\Omega$  for VBs with TianQin, LISA, Taiji, DECIGO and the network of all them.

Source	parameters	$\Delta\theta$								
		TQ	LISA	Taiji	DECIGO	TL	TD	LD	TLD	TLTD
J0806	$M_c = 0.331 (M_\odot)$	0.00166	0.00110	5.48e-4	1.65e-4	5.85e-4	1.50e-5	1.50e-5	1.50e-5	1.48e-5
	$d = 5.000 (kpc)$	0.330	0.349	0.173	0.395	0.165	0.0934	0.0896	0.0756	0.0523
	$\iota = 38 (deg)$	0.154	0.102	0.0510	0.0154	2.70	1.79	1.71	1.42	0.955
	$\Omega (deg^2)$	0.00919	0.00437	0.00108	2.49e-4	0.00126	2.10e-5	2.00e-5	1.66e-5	1.15e-5
ATLAS J1013	$M_c = 0.232 (M_\odot)$	0.0491	0.0188	0.0128	0.00505	0.0122	4.72e-4	4.80e-4	4.68e-4	4.59e-4
	$d = 1.802 (kpc)$	0.639	0.245	0.167	0.0664	0.159	0.00739	0.00742	0.00731	0.00715
	$\iota = 82 (deg)$	1.257	0.854	0.559	0.486	0.465	0.0982	0.158	0.0966	0.0934
	$\Omega (deg^2)$	0.00207	0.0995	0.0689	0.0221	9.88e-5	8.11e-5	0.00239	8.06e-5	7.94e-5
V407 Vul	$M_c = 0.311 (M_\odot)$	0.0437	0.0129	0.0105	0.00456	0.00865	3.96e-4	3.91e-4	3.91e-4	3.83e-4
	$d = 2.087 (kpc)$	0.508	0.154	0.125	0.0554	0.103	0.00904	0.00888	0.00886	0.00860
	$\iota = 60 (deg)$	2.89	0.854	0.698	0.302	0.812	0.173	0.170	0.170	0.164
	$\Omega (deg^2)$	3.59e-4	0.0995	0.0664	1.66e-6	0.00808	1.53e-5	1.53e-5	1.53e-5	1.53e-5
ES Cet	$M_c = 0.295 (M_\odot)$	–	0.0149	0.0147	0.00601	0.0104	5.87e-4	5.78e-4	5.78e-4	5.69e-4
	$d = 1.727 (kpc)$	–	0.156	0.154	0.0642	0.109	0.0110	0.0104	0.0103	0.00994
	$\iota = 60 (deg)$	–	0.984	0.970	0.397	1.23	0.348	0.313	0.311	0.287
	$\Omega (deg^2)$	–	0.0200	0.0195	0.0113	0.00846	0.00138	0.00113	0.00111	9.28e-4
ZTF J0127	$M_c = 0.315 (M_\odot)$	–	0.0969	0.175	0.0434	0.0667	0.00357	0.00349	0.00349	0.00347
	$d = 1.283 (kpc)$	–	0.659	1.19	0.296	0.454	0.0250	0.0245	0.0245	0.0243
	$\iota = 80 (deg)$	–	5.63	10.2	2.53	0.527	0.128	0.124	0.124	0.123
	$\Omega (deg^2)$	–	0.287	0.935	3.04e-5	0.118	8.86e-4	8.46e-4	8.45e-4	8.33e-4
SDSS J1351	$M_c = 0.224 (M_\odot)$	–	0.323	–	0.130	0.226	0.0120	0.0118	0.0118	0.0118
	$d = 1.341 (kpc)$	–	3.22	–	1.37	2.26	0.209	0.126	0.126	0.124
	$\iota = 60 (deg)$	–	21.4	–	8.61	3.03	13.0	2.23	2.22	2.05
	$\Omega (deg^2)$	–	0.370	–	0.916	0.139	0.0865	0.00570	0.00563	0.00531
AM CVn	$M_c = 0.238 (M_\odot)$	0.527	0.0814	0.176	0.0324	0.0563	0.00311	0.00306	0.00305	0.00304
	$d = 0.302 (kpc)$	1.12	0.173	0.375	0.0685	0.120	0.00683	0.00673	0.00672	0.00670
	$\iota = 43 (deg)$	44.3	6.84	14.8	2.72	2.39	0.518	0.505	0.505	0.502
	$\Omega (deg^2)$	1.46e-4	0.0458	0.215	2.58e-5	0.00416	4.17e-5	4.03e-5	4.02e-5	3.99e-5
SDSS J1908	$M_c = 0.204 (M_\odot)$	–	0.611	–	0.193	0.414	0.0163	0.0161	0.0161	0.0161
	$d = 0.977 (kpc)$	–	5.26	–	1.73	3.57	0.316	0.310	0.309	0.308
	$\iota = 15 (deg)$	–	–	–	42.6	–	61.8	60.6	60.5	60.2
	$\Omega (deg^2)$	–	3.91	–	9.86e-6	0.564	5.54e-6	5.54e-6	5.54e-6	5.54e-6
HP Lib	$M_c = 0.164 (M_\odot)$	–	0.302	0.654	0.107	0.208	0.00979	0.00971	0.00965	0.00962
	$d = 0.280 (kpc)$	–	0.864	1.87	0.345	0.596	0.0572	0.0368	0.0359	0.0348
	$\iota = 30 (deg)$	–	34.6	74.9	12.3	18.6	20.3	9.73	9.45	8.86
	$\Omega (deg^2)$	–	0.0760	0.356	0.0394	0.00220	8.45e-4	0.00105	4.06e-4	3.89e-4
TIC378898110	$M_c = 0.224 (M_\odot)$	–	1.65	–	0.438	1.11	0.0352	0.0349	0.0349	0.0348
	$d = 0.309 (kpc)$	–	3.79	–	1.01	2.55	0.0808	0.0802	0.0801	0.0800
	$\iota = 74 (deg)$	–	–	–	26.1	1.68	0.230	0.227	0.227	0.227
	$\Omega (deg^2)$	–	3.85	–	2.14e-5	1.79	6.79e-4	6.71e-4	6.71e-4	6.69e-4
CXOGBS J1751	$M_c = 0.173 (M_\odot)$	–	–	–	1.96	–	0.168	0.167	0.166	0.165
	$d = 0.939 (kpc)$	–	–	–	17.7	–	1.51	1.50	1.49	1.49
	$\iota = 60 (deg)$	–	–	–	–	–	13.3	10.4	9.17	8.68
	$\Omega (deg^2)$	–	–	–	5.28	–	0.345	0.229	0.191	0.176
CR Boo	$M_c = 0.184 (M_\odot)$	–	2.16	–	0.593	1.50	0.0584	0.0579	0.0578	0.0576
	$d = 0.352 (kpc)$	–	6.92	–	1.90	4.80	0.192	0.189	0.189	0.188
	$\iota = 30 (deg)$	–	–	–	67.9	59.1	12.2	11.0	10.8	10.6
	$\Omega (deg^2)$	–	2.29	–	0.511	0.258	0.0522	0.0500	0.0417	0.0398
V803 Cen	$M_c = 0.220 (M_\odot)$	–	2.33	–	0.603	1.58	0.0476	0.0471	0.0471	0.0469
	$d = 0.287 (kpc)$	–	5.07	–	1.32	3.46	0.122	0.119	0.119	0.119
	$\iota = 14 (deg)$	–	–	–	–	–	55.8	54.2	54.2	53.9
	$\Omega (deg^2)$	–	0.0264	–	0.00267	0.0131	3.41e-4	2.17e-4	2.17e-4	2.01e-4
SMSS J1138	$M_c = 0.405 (M_\odot)$	–	–	–	0.912	–	0.0778	0.0773	0.0773	0.0771
	$d = 0.547 (kpc)$	–	–	–	2.05	–	0.175	0.174	0.174	0.174
	$\iota = 89 (deg)$	–	–	–	52.3	–	0.201	0.200	0.200	0.199
	$\Omega (deg^2)$	–	–	–	0.0448	–	0.0435	0.0422	0.0421	0.0417
ZTF J1539	$M_c = 0.303 (M_\odot)$	0.0134	0.00280	0.00154	5.52e-4	0.00190	5.43e-5	5.41e-5	5.41e-5	5.34e-5

*Continued on next page*

TABLE V – *Continued from previous page*

Source	parameters	$\Delta\theta$								
		TQ	LISA	Taiji	DECIGO	TL	TD	LD	TLD	TLTD
ZTF J0546	$d = 1.629$ (kpc)	0.140	0.0291	0.0160	0.00583	0.0197	0.00120	0.00119	0.00119	0.00117
	$\iota = 84$ (deg)	0.774	0.161	0.0886	0.0318	0.230	0.0271	0.0270	0.0270	0.0264
	$\Omega$ (deg <sup>2</sup> )	0.329	0.0414	0.0125	4.85e-6	0.00579	4.54e-7	4.54e-7	4.54e-7	4.54e-7
	$M_c = 0.365$ ( $M_\odot$ )	0.0170	0.00519	0.00321	0.00173	0.00340	1.40e-4	1.41e-4	1.39e-4	1.35e-4
ZTF J1858	$d = 3.707$ (kpc)	0.353	0.129	0.0800	0.0628	0.0815	0.0127	0.0163	0.0124	0.0116
	$\iota = 60$ (deg)	1.12	0.343	0.213	0.114	0.775	0.208	0.326	0.201	0.186
	$\Omega$ (deg <sup>2</sup> )	3.11e-5	0.0380	0.0146	0.00857	4.90e-5	4.64e-5	7.35e-4	4.58e-5	4.44e-5
	$M_c = 0.365$ ( $M_\odot$ )	0.0190	0.00610	0.00424	0.00214	0.00397	1.90e-4	1.90e-4	1.88e-4	1.84e-4
ZTF J2243	$d = 2.895$ (kpc)	0.283	0.107	0.0741	0.408	0.0666	0.0431	0.0301	0.0269	0.0181
	$\iota = 60$ (deg)	1.25	0.404	0.281	0.141	0.778	1.05	0.695	0.609	0.402
	$\Omega$ (deg <sup>2</sup> )	1.65e-6	0.00728	0.00352	0.0102	5.00e-5	1.07e-5	5.62e-5	8.17e-6	7.46e-6
	$M_c = 0.286$ ( $M_\odot$ )	0.0668	0.0118	0.00839	0.00401	0.00808	3.32e-4	3.29e-4	3.28e-4	3.22e-4
SDSS J0651	$d = 1.753$ (kpc)	0.690	0.123	0.0873	0.0418	0.0840	0.00452	0.00447	0.00447	0.00436
	$\iota = 82$ (deg)	3.86	0.684	0.486	0.232	0.358	0.0549	0.0543	0.0543	0.0531
	$\Omega$ (deg <sup>2</sup> )	0.454	0.108	0.0542	8.69e-6	0.0387	7.86e-7	7.86e-7	7.86e-7	7.85e-7
	$M_c = 0.311$ ( $M_\odot$ )	0.167	0.0336	0.0534	0.0166	0.0228	0.00140	0.00139	0.00137	0.00136
ZTF J0538	$d = 0.958$ (kpc)	0.861	0.173	0.275	0.0872	0.118	0.00834	0.00772	0.00765	0.00751
	$\iota = 87$ (deg)	9.60	1.93	3.06	0.955	0.318	0.280	0.279	0.209	0.193
	$\Omega$ (deg <sup>2</sup> )	4.34e-4	0.0416	0.105	0.115	2.27e-4	2.01e-4	0.00134	1.87e-4	1.84e-4
	$M_c = 0.329$ ( $M_\odot$ )	–	0.0645	0.125	0.0304	0.0445	0.00274	0.00269	0.00268	0.00267
ZTF J1905	$d = 0.997$ (kpc)	–	0.326	0.631	0.162	0.225	0.0168	0.0146	0.0145	0.0142
	$\iota = 85$ (deg)	–	3.71	7.18	1.75	0.556	1.03	0.525	0.471	0.429
	$\Omega$ (deg <sup>2</sup> )	–	0.0606	0.227	0.0486	0.00305	0.00100	0.00129	6.32e-4	6.10e-4
	$M_c = 0.365$ ( $M_\odot$ )	0.465	0.124	0.268	0.0440	0.0837	0.00374	0.00370	0.00369	0.00368
SDSS J0935	$d = 0.696$ (kpc)	1.48	0.394	0.854	0.140	0.267	0.0123	0.0121	0.0121	0.0121
	$\iota = 60$ (deg)	30.7	8.19	17.7	2.91	1.01	0.192	0.190	0.189	0.189
	$\Omega$ (deg <sup>2</sup> )	0.00130	0.441	2.07	1.62e-6	0.0393	6.37e-5	6.32e-5	6.31e-5	6.30e-5
	$M_c = 0.413$ ( $M_\odot$ )	0.408	0.125	0.265	0.0447	0.0800	0.00354	0.00351	0.00350	0.00349
SDSS J2322	$d = 0.396$ (kpc)	0.651	0.199	0.423	0.0713	0.128	0.00572	0.00566	0.00564	0.00563
	$\iota = 60$ (deg)	27.0	8.25	17.5	2.96	0.763	0.153	0.147	0.146	0.145
	$\Omega$ (deg <sup>2</sup> )	3.75e-5	0.0161	0.0727	9.78e-7	0.00146	4.00e-5	3.37e-5	3.33e-5	3.22e-5
	$M_c = 0.261$ ( $M_\odot$ )	–	0.541	–	0.198	0.364	0.0177	0.0175	0.0175	0.0174
PTF J0533	$d = 0.860$ (kpc)	–	2.98	–	1.30	2.01	0.234	0.177	0.170	0.164
	$\iota = 27$ (deg)	–	68.2	–	25.0	42.9	31.3	22.2	20.8	19.8
	$\Omega$ (deg <sup>2</sup> )	–	0.573	–	0.225	0.00805	0.00420	0.0112	0.00252	0.00238
	$M_c = 0.275$ ( $M_\odot$ )	–	–	–	0.471	–	0.0454	0.0465	0.0450	0.0449
ZTF J2029	$d = 1.172$ (kpc)	–	–	–	3.34	–	0.324	0.330	0.320	0.320
	$\iota = 73$ (deg)	–	–	–	28.2	–	0.952	0.885	0.841	0.823
	$\Omega$ (deg <sup>2</sup> )	–	–	–	1.18	–	0.0502	0.117	0.0424	0.0411
	$M_c = 0.270$ ( $M_\odot$ )	–	–	–	0.685	–	0.0639	0.0634	0.0633	0.0632
J1239	$d = 1.095$ (kpc)	–	–	–	4.63	–	0.433	0.430	0.429	0.428
	$\iota = 87$ (deg)	–	–	–	39.3	–	0.379	0.374	0.372	0.371
	$\Omega$ (deg <sup>2</sup> )	–	–	–	0.00235	–	0.0514	0.0473	0.0467	0.0458
	$M_c = 0.381$ ( $M_\odot$ )	–	–	–	0.358	–	0.0311	0.0309	0.0309	0.0308
ZTF J0722	$d = 0.972$ (kpc)	–	–	–	1.52	–	0.133	0.133	0.132	0.132
	$\iota = 71$ (deg)	–	–	–	21.7	–	1.13	1.01	0.946	0.915
	$\Omega$ (deg <sup>2</sup> )	–	–	–	0.503	–	0.0442	0.0473	0.0348	0.0332
	$M_c = 0.308$ ( $M_\odot$ )	–	–	–	1.38	–	0.125	0.124	0.124	0.123
ZTF J1749	$d = 1.267$ (kpc)	–	–	–	9.47	–	0.856	0.850	0.848	0.846
	$\iota = 90$ (deg)	–	–	–	79.1	–	0.490	0.486	0.485	0.483
	$\Omega$ (deg <sup>2</sup> )	–	–	–	0.473	–	0.377	0.362	0.358	0.354
	$M_c = 0.290$ ( $M_\odot$ )	–	–	–	–	–	–	0.276	0.275	0.274
SDSS J0634	$d = 1.291$ (kpc)	–	–	–	–	–	–	2.04	2.04	2.03
	$\iota = 86$ (deg)	–	–	–	–	–	–	0.756	0.744	0.743
	$\Omega$ (deg <sup>2</sup> )	–	–	–	–	–	–	0.147	0.0577	0.0575
	$M_c = 0.264$ ( $M_\odot$ )	–	2.35	–	0.668	1.46	0.0545	0.0548	0.0541	0.0540
SDSS J0634	$d = 0.435$ (kpc)	–	6.46	–	1.84	4.01	0.150	0.152	0.149	0.148
	$\iota = 43$ (deg)	–	–	–	56.1	11.6	2.62	3.93	2.57	2.55

*Continued on next page*

TABLE V – *Continued from previous page*

Source	parameters	$\Delta\theta$								
		TQ	LISA	Taiji	DECIGO	TL	TD	LD	TLD	TLTD
	$\Omega$ (deg <sup>2</sup> )	–	2.45	–	0.653	6.24e-5	6.21e-5	0.0542	6.20e-5	6.20e-5
SMSS J0338	$M_c = 0.256$ ( $M_\odot$ )	–	–	–	2.96	–	0.250	0.249	0.249	0.249
	$d = 0.536$ (kpc)	–	–	–	10.3	–	0.874	0.871	0.870	0.869
	$\iota = 69$ (deg)	–	–	–	–	–	0.826	0.822	0.822	0.820
	$\Omega$ (deg <sup>2</sup> )	–	–	–	2.47e-4	–	1.73e-5	1.73e-5	1.73e-5	1.73e-5
SDSS J1630	$M_c = 0.406$ ( $M_\odot$ )	–	–	–	7.35	–	0.705	0.702	0.702	0.701
	$d = 0.848$ (kpc)	–	–	–	25.6	–	2.46	2.45	2.45	2.44
	$\iota = 60$ (deg)	–	–	–	–	–	2.15	2.13	2.13	2.12
	$\Omega$ (deg <sup>2</sup> )	–	–	–	2.21e-4	–	0.00748	0.00746	0.00746	0.00745
J1526	$M_c = 0.335$ ( $M_\odot$ )	–	–	–	9.76	–	0.845	0.833	0.832	0.829
	$d = 0.625$ (kpc)	–	–	–	30.4	–	2.62	2.59	2.58	2.58
	$\iota = 60$ (deg)	–	–	–	–	–	12.2	7.01	6.89	6.23
	$\Omega$ (deg <sup>2</sup> )	–	–	–	9.57	–	0.298	0.478	0.162	0.146
ZTF J0526	$M_c = 0.365$ ( $M_\odot$ )	–	0.488	–	0.175	0.322	0.0130	0.0128	0.0128	0.0128
	$d = 0.845$ (kpc)	–	1.88	–	0.674	1.24	0.0504	0.0500	0.0499	0.0498
	$\iota = 60$ (deg)	–	32.3	–	11.5	2.34	0.404	0.399	0.398	0.397
	$\Omega$ (deg <sup>2</sup> )	–	0.530	–	1.03e-5	0.0350	5.11e-7	5.12e-7	5.11e-7	5.11e-7
ZTF J1840	$M_c = 0.365$ ( $M_\odot$ )	–	–	–	4.57	–	0.411	0.410	0.408	0.407
	$d = 1.286$ (kpc)	–	–	–	26.9	–	2.43	2.42	2.40	2.39
	$\iota = 60$ (deg)	–	–	–	–	–	13.4	11.0	9.23	8.61
	$\Omega$ (deg <sup>2</sup> )	–	–	–	21.1	–	0.0439	0.326	0.0292	0.0273
ZTF J1611	$M_c = 0.365$ ( $M_\odot$ )	–	–	–	10.5	–	0.989	0.985	0.985	0.983
	$d = 0.257$ (kpc)	–	–	–	12.4	–	1.16	1.16	1.16	1.15
	$\iota = 60$ (deg)	–	–	–	–	–	1.13	1.13	1.13	1.12
	$\Omega$ (deg <sup>2</sup> )	–	–	–	1.06e-4	–	0.00831	0.00830	0.00830	0.00830
ZTF J2334	$M_c = 0.365$ ( $M_\odot$ )	–	–	–	96.2	–	7.85	7.76	7.76	7.71
	$d = 0.076$ (kpc)	–	–	–	33.4	–	2.72	2.69	2.69	2.67
	$\iota = 60$ (deg)	–	–	–	–	–	1.53	1.50	1.50	1.48
	$\Omega$ (deg <sup>2</sup> )	–	–	–	1.01e-4	–	0.0139	0.0133	0.0132	0.0129
ZTF J2007	$M_c = 0.365$ ( $M_\odot$ )	–	–	–	55.8	–	4.88	4.84	4.83	4.80
	$d = 0.045$ (kpc)	–	–	–	11.5	–	1.00	0.994	0.992	0.986
	$\iota = 60$ (deg)	–	–	–	–	–	0.864	0.887	0.852	0.845
	$\Omega$ (deg <sup>2</sup> )	–	–	–	4.41e-5	–	4.52e-5	0.00345	4.52e-5	4.52e-5
1RXS J1718	$M_c = 0.365$ ( $M_\odot$ )	0.0142	0.00497	0.00274	0.00132	0.00320	1.06e-4	1.07e-4	1.06e-4	1.04e-4
	$d = 6.500$ (kpc)	0.646	0.294	0.162	0.114	0.183	0.0350	0.0345	0.0326	0.0285
	$\iota = 60$ (deg)	0.939	0.329	0.181	0.0875	1.20	0.391	0.378	0.354	0.289
	$\Omega$ (deg <sup>2</sup> )	8.26e-5	0.0273	0.00832	0.00520	0.00128	3.21e-4	5.64e-4	2.86e-4	2.25e-4
4U 1820-30	$M_c = 0.228$ ( $M_\odot$ )	–	–	–	0.106	–	0.00906	0.00888	0.00883	0.00872
	$d = 7.972$ (kpc)	–	–	–	7.61	–	0.995	0.836	0.776	0.722
	$\iota = 60$ (deg)	–	–	–	7.03	–	9.87	6.57	5.87	5.09
	$\Omega$ (deg <sup>2</sup> )	–	–	–	1.44	–	0.0172	0.0568	0.0102	0.00909
4U 0513-40	$M_c = 0.500$ ( $M_\odot$ )	–	–	–	0.164	–	0.0151	0.0149	0.0149	0.0148
	$d = 6.466$ (kpc)	–	–	–	3.56	–	0.360	0.354	0.354	0.353
	$\iota = 60$ (deg)	–	–	–	10.9	–	1.19	1.17	1.16	1.16
	$\Omega$ (deg <sup>2</sup> )	–	–	–	9.77e-5	–	4.56e-6	4.56e-6	4.56e-6	4.56e-6

- [1] A. Einstein, Naherungsweise Integration der Feldgleichungen der Gravitation, Sitzungsberichte der Koniglich Preussischen Akademie der Wissenschaften , 688 (1916).  
[2] K. S. Thorne, Multipole expansions of gravitational radiation, *Rev. Mod. Phys.* **52**, 299 (1980).  
[3] J. H. Taylor and J. M. Weisberg, A new test of general relativity - Gravitational radiation and the binary pulsar

- PSR 1913+16, *Astrophysical Journal* **253**, 908 (1982).  
[4] B. F. Schutz, Determining the Hubble constant from gravitational wave observations, *Nature* **323**, 310 (1986).  
[5] LIGO Scientific Collaboration *et al.*, Advanced LIGO, *Classical and Quantum Gravity* **32**, 074001 (2015), [arXiv:1411.4547 \[gr-qc\]](https://arxiv.org/abs/1411.4547).  
[6] F. Acernese *et al.*, Advanced Virgo: a second-generation

- interferometric gravitational wave detector, *Classical and Quantum Gravity* **32**, 024001 (2015), [arXiv:1408.3978 \[gr-qc\]](#).
- [7] B. P. Abbott *et al.*, Prospects for observing and localizing gravitational-wave transients with Advanced LIGO, Advanced Virgo and KAGRA, *Living Reviews in Relativity* **23**, 3 (2020).
- [8] B. P. Abbott *et al.*, Observation of Gravitational Waves from a Binary Black Hole Merger, *Phys. Rev. Lett* **116**, 061102 (2016), [arXiv:1602.03837 \[gr-qc\]](#).
- [9] K. Somiya, Detector configuration of KAGRA—the Japanese cryogenic gravitational-wave detector, *Classical and Quantum Gravity* **29**, 124007 (2012), [arXiv:1111.7185 \[gr-qc\]](#).
- [10] B. P. Abbott *et al.*, GWTC-1: A Gravitational-Wave Transient Catalog of Compact Binary Mergers Observed by LIGO and Virgo during the First and Second Observing Runs, *Physical Review X* **9**, 031040 (2019), [arXiv:1811.12907 \[astro-ph.HE\]](#).
- [11] R. Abbott *et al.*, GWTC-2: Compact Binary Coalescences Observed by LIGO and Virgo during the First Half of the Third Observing Run, *Physical Review X* **11**, 021053 (2021), [arXiv:2010.14527 \[gr-qc\]](#).
- [12] R. Abbott *et al.*, Observation of Gravitational Waves from Two Neutron Star-Black Hole Coalescences, *Astrophysical Journal* **915**, L5 (2021), [arXiv:2106.15163 \[astro-ph.HE\]](#).
- [13] R. Abbott, *et al.*, GWTC-3: Compact Binary Coalescences Observed by LIGO and Virgo during the Second Part of the Third Observing Run, *Physical Review X* **13**, 041039 (2023), [arXiv:2111.03606 \[gr-qc\]](#).
- [14] R. Abbott *et al.*, GWTC-2.1: Deep extended catalog of compact binary coalescences observed by LIGO and Virgo during the first half of the third observing run, *Phys. Rev. D* **109**, 022001 (2024), [arXiv:2108.01045 \[gr-qc\]](#).
- [15] A. G. Abac *et al.*, Observation of Gravitational Waves from the Coalescence of a 2.5–4.5  $M_{\odot}$  Compact Object and a Neutron Star, *Astrophysical Journal* **970**, L34 (2024), [arXiv:2404.04248 \[astro-ph.HE\]](#).
- [16] S. T. McWilliams, R. Caldwell, K. Holley-Bockelmann, S. L. Larson, and M. Vallisneri, Astro2020 Decadal Science White Paper: The state of gravitational-wave astrophysics in 2020, *arXiv e-prints*, [arXiv:1903.04592 \(2019\)](#), [arXiv:1903.04592 \[astro-ph.HE\]](#).
- [17] M. Kamionkowski and E. D. Kovetz, The quest for b modes from inflationary gravitational waves, *Annual Review of Astronomy and Astrophysics* **54**, 227 (2016).
- [18] Z. Arzoumanian *et al.*, The NANOGrav 11 Year Data Set: Pulsar-timing Constraints on the Stochastic Gravitational-wave Background, *Astrophysical Journal* **859**, 47 (2018), [arXiv:1801.02617 \[astro-ph.HE\]](#).
- [19] R. M. Shannon *et al.*, Gravitational waves from binary supermassive black holes missing in pulsar observations, *Science* **349**, 1522 (2015), [arXiv:1509.07320 \[astro-ph.CO\]](#).
- [20] P. Amaro-Seoane *et al.*, Laser Interferometer Space Antenna, *arXiv e-prints*, [arXiv:1702.00786 \(2017\)](#), [arXiv:1702.00786 \[astro-ph.IM\]](#).
- [21] J. Luo *et al.*, TianQin: a space-borne gravitational wave detector, *Classical and Quantum Gravity* **33**, 035010 (2016), [arXiv:1512.02076 \[astro-ph.IM\]](#).
- [22] A. Klein, E. Barausse, A. Sesana, A. Petiteau, E. Berti, S. Babak, J. Gair, S. Aoudia, I. Hinder, F. Ohme, and B. Wardell, Science with the space-based interferometer elisa: Supermassive black hole binaries, *Phys. Rev. D* **93**, 024003 (2016).
- [23] J. Magorrian, S. Tremaine, D. Richstone, R. Bender, G. Bower, A. Dressler, S. M. Faber, K. Gebhardt, R. Green, C. Grillmair, J. Kormendy, and T. Lauer, The Demography of Massive Dark Objects in Galaxy Centers, *Astronomical Journal* **115**, 2285 (1998), [arXiv:astro-ph/9708072 \[astro-ph\]](#).
- [24] D. Lynden-Bell, Galactic Nuclei as Collapsed Old Quasars, *Nature* **223**, 690 (1969).
- [25] S. Babak, J. Gair, A. Sesana, E. Barausse, C. F. Sopuerta, C. P. L. Berry, E. Berti, P. Amaro-Seoane, A. Petiteau, and A. Klein, Science with the space-based interferometer LISA. V. Extreme mass-ratio inspirals, *Phys. Rev. D* **95**, 103012 (2017), [arXiv:1703.09722 \[gr-qc\]](#).
- [26] H.-M. Fan, Y.-M. Hu, E. Barausse, A. Sesana, J.-d. Zhang, X. Zhang, T.-G. Zi, and J. Mei, Science with the tianqin observatory: Preliminary result on extreme-mass-ratio inspirals, *Phys. Rev. D* **102**, 063016 (2020).
- [27] A. Lamberts, S. Garrison-Kimmel, P. F. Hopkins, E. Quataert, J. S. Bullock, C.-A. Faucher-Giguère, A. Wetzel, D. Kereš, K. Drango, and R. E. Sanderson, Predicting the binary black hole population of the Milky Way with cosmological simulations, *MNRAS* **480**, 2704 (2018), [arXiv:1801.03099 \[astro-ph.GA\]](#).
- [28] V. Korol, E. M. Rossi, P. J. Groot, G. Nelemans, S. Toonen, and A. G. A. Brown, Prospects for detection of detached double white dwarf binaries with Gaia, LSST and LISA, *MNRAS* **470**, 1894 (2017), [arXiv:1703.02555 \[astro-ph.HE\]](#).
- [29] T. Robson, N. J. Cornish, N. Tamanini, and S. Toonen, Detecting hierarchical stellar systems with LISA, *Phys. Rev. D* **98**, 064012 (2018), [arXiv:1806.00500 \[gr-qc\]](#).
- [30] M. Y. M. Lau, I. Mandel, A. Vigna-Gómez, C. J. Neijssel, S. Stevenson, and A. Sesana, Detecting double neutron stars with LISA, *MNRAS* **492**, 3061 (2020), [arXiv:1910.12422 \[astro-ph.HE\]](#).
- [31] J. D. Romano and N. J. Cornish, Detection methods for stochastic gravitational-wave backgrounds: a unified treatment, *Living Reviews in Relativity* **20**, 2 (2017), [arXiv:1608.06889 \[gr-qc\]](#).
- [32] N. Tamanini and C. Danielski, The gravitational-wave detection of exoplanets orbiting white dwarf binaries using LISA, *Nature Astronomy* **3**, 858 (2019), [arXiv:1812.04330 \[astro-ph.EP\]](#).
- [33] E. Berti, A. Buonanno, and C. M. Will, Estimating spinning binary parameters and testing alternative theories of gravity with lisa, *Phys. Rev. D* **71**, 084025 (2005).
- [34] G. Nelemans, L. R. Yungelson, and S. F. Portegies Zwart, The gravitational wave signal from the Galactic disk population of binaries containing two compact objects, *A&A* **375**, 890 (2001), [arXiv:astro-ph/0105221 \[astro-ph\]](#).
- [35] S. Yu and C. S. Jeffery, The gravitational wave signal from diverse populations of double white dwarf binaries in the Galaxy, *A&A* **521**, A85 (2010), [arXiv:1007.4267 \[astro-ph.SR\]](#).
- [36] S.-J. Huang, Y.-M. Hu, V. Korol, P.-C. Li, Z.-C. Liang, Y. Lu, H.-T. Wang, S. Yu, and J. Mei, Science with the TianQin Observatory: Preliminary results on Galactic double white dwarf binaries, *Phys. Rev. D* **102**, 063021 (2020), [arXiv:2005.07889 \[astro-ph.HE\]](#).

- [37] A. Stroerer and A. Vecchio, The LISA verification binaries, *Classical and Quantum Gravity* **23**, S809 (2006), [arXiv:astro-ph/0605227 \[astro-ph\]](#).
- [38] T. Kupfer, V. Korol, S. Shah, G. Nelemans, T. R. Marsh, G. Ramsay, P. J. Groot, D. T. H. Steeghs, and E. M. Rossi, LISA verification binaries with updated distances from Gaia Data Release 2, *MNRAS* **480**, 302 (2018), [arXiv:1805.00482 \[astro-ph.SR\]](#).
- [39] D. Hils, P. L. Bender, and R. F. Webbink, Gravitational Radiation from the Galaxy, *Astrophysical Journal* **360**, 75 (1990).
- [40] P. Amaro-Seoane *et al.*, Astrophysics with the Laser Interferometer Space Antenna, *Living Reviews in Relativity* **26**, 2 (2023), [arXiv:2203.06016 \[gr-qc\]](#).
- [41] B. Warner, The AM Canum Venaticorum Stars, *Astrophysics and Space Science* **225**, 249 (1995).
- [42] J.-E. Solheim, AM CVn Stars: Status and Challenges, *PASP* **122**, 1133 (2010).
- [43] E.-K. Li *et al.*, Gravitational wave astronomy with TianQin, *Reports on Progress in Physics* **88**, 056901 (2025), [arXiv:2409.19665 \[astro-ph.GA\]](#).
- [44] L. Ren, C. Li, B. Ma, S. Cheng, S.-J. Huang, B. Tang, and Y.-m. Hu, A Systematic Search for Short-period Close White Dwarf Binary Candidates Based on Gaia EDR3 Catalog and Zwicky Transient Facility Data, *ApJS* **264**, 39 (2023), [arXiv:2302.02802 \[astro-ph.SR\]](#).
- [45] U. Heber, Hot Subluminous Stars, *PASP* **128**, 082001 (2016), [arXiv:1604.07749 \[astro-ph.SR\]](#).
- [46] C. Knigge, I. Baraffe, and J. Patterson, The Evolution of Cataclysmic Variables as Revealed by Their Donor Stars, *ApJS* **194**, 28 (2011), [arXiv:1102.2440 \[astro-ph.SR\]](#).
- [47] S. Rappaport, P. C. Joss, and R. F. Webbink, The evolution of highly compact binary stellar systems., *Astrophysical Journal* **254**, 616 (1982).
- [48] M. Armas Padilla, J. M. Corral-Santana, A. Borghese, V. A. Cúneo, T. Muñoz-Darias, J. Casares, and M. A. P. Torres, UltraCompCAT: A comprehensive catalogue of ultra-compact and short orbital period X-ray binaries, *A&A* **677**, A186 (2023), [arXiv:2305.07691 \[astro-ph.HE\]](#).
- [49] J. J. M. in't Zand, P. G. Jonker, C. G. Bassa, C. B. Markwardt, and A. M. Levine, Monitoring campaign of 1RXS J171824.2-402934, the low-mass X-ray binary with the lowest mass accretion rate, *A&A* **506**, 857 (2009), [arXiv:0905.2519 \[astro-ph.HE\]](#).
- [50] W.-C. Chen, D.-D. Liu, and B. Wang, Detectability of Ultra-compact X-Ray Binaries as LISA Sources, *Astrophysical Journal* **900**, L8 (2020), [arXiv:2008.05143 \[astro-ph.HE\]](#).
- [51] T. Kupfer, V. Korol, T. B. Littenberg, S. Shah, E. Savalle, P. J. Groot, T. R. Marsh, M. Le Jeune, G. Nelemans, A. F. Pala, A. Petiteau, G. Ramsay, D. Steeghs, and S. Babak, LISA Galactic Binaries with Astrometry from Gaia DR3, *Astrophysical Journal* **963**, 100 (2024), [arXiv:2302.12719 \[astro-ph.SR\]](#).
- [52] S. Vennes, A. Kawka, S. J. O'Toole, P. Németh, and D. Burton, The Shortest Period sdB Plus White Dwarf Binary CD-30 11223 (GALEX J1411-3053), *Astrophysical Journal* **759**, L25 (2012), [arXiv:1210.1512 \[astro-ph.SR\]](#).
- [53] S. Geier, T. R. Marsh, B. Wang, B. Dunlap, B. N. Barlow, V. Schaffenroth, X. Chen, A. Irrgang, P. F. L. Maxted, E. Ziegerer, T. Kupfer, B. Miszalski, U. Heber, Z. Han, A. Shporer, J. H. Telling, B. T. Gänsicke, R. H. Østensen, S. J. O'Toole, and R. Napiwotzki, A progenitor binary and an ejected mass donor remnant of faint type Ia supernovae, *A&A* **554**, A54 (2013), [arXiv:1304.4452 \[astro-ph.SR\]](#).
- [54] T. Kupfer *et al.*, The OmegaWhite Survey for Short-period Variable Stars. V. Discovery of an Ultracompact Hot Subdwarf Binary with a Compact Companion in a 44-minute Orbit, *Astrophysical Journal* **851**, 28 (2017), [arXiv:1710.07287 \[astro-ph.SR\]](#).
- [55] T. Kupfer *et al.*, A New Class of Roche Lobe-filling Hot Subdwarf Binaries, *Astrophysical Journal* **898**, L25 (2020), [arXiv:2007.05349 \[astro-ph.SR\]](#).
- [56] J. Mei *et al.*, The TianQin project: Current progress on science and technology, *Progress of Theoretical and Experimental Physics* **2021**, 05A107 (2021), [arXiv:2008.10332 \[gr-qc\]](#).
- [57] P. C. Peters and J. Mathews, Gravitational radiation from point masses in a keplerian orbit, *Phys. Rev.* **131**, 435 (1963).
- [58] L. D. Landau and E. M. Lifshitz, *The classical theory of fields; 2nd ed.*, Course of theoretical physics (Pergamon, London, 1962) trans. from the Russian.
- [59] C. Cutler, Angular resolution of the lisa gravitational wave detector, *Phys. Rev. D* **57**, 7089 (1998).
- [60] S. Babak, M. Hewitson, and A. Petiteau, LISA Sensitivity and SNR Calculations, *arXiv e-prints*, [arXiv:2108.01167 \(2021\)](#), [arXiv:2108.01167 \[astro-ph.IM\]](#).
- [61] F. Huang, Z.-C. Chen, and Q.-G. Huang, Detecting Cosmological Phase Transitions with Taiji: Sensitivity Analysis and Parameter Estimation, *arXiv e-prints*, [arXiv:2504.16712 \(2025\)](#), [arXiv:2504.16712 \[gr-qc\]](#).
- [62] K. Yagi and N. Seto, Detector configuration of DECIGO/BBO and identification of cosmological neutron-star binaries, *Phys. Rev. D* **83**, 044011 (2011), [arXiv:1101.3940 \[astro-ph.CO\]](#).
- [63] S. Shah, M. van der Sluys, and G. Nelemans, Using electromagnetic observations to aid gravitational-wave parameter estimation of compact binaries observed with LISA, *A&A* **544**, A153 (2012), [arXiv:1207.6770 \[astro-ph.IM\]](#).
- [64] C. Cutler, Angular resolution of the LISA gravitational wave detector, *Phys. Rev. D* **57**, 7089 (1998), [arXiv:gr-qc/9703068 \[gr-qc\]](#).
- [65] P. Amaro Seoane *et al.*, The effect of mission duration on LISA science objectives, *General Relativity and Gravitation* **54**, 3 (2022), [arXiv:2107.09665 \[astro-ph.IM\]](#).
- [66] G. H. A. Roelofs, A. Rau, T. R. Marsh, D. Steeghs, P. J. Groot, and G. Nelemans, Spectroscopic Evidence for a 5.4 Minute Orbital Period in HM Cancri, *Astrophysical Journal* **711**, L138 (2010), [arXiv:1003.0658 \[astro-ph.SR\]](#).
- [67] E. T. Chickles *et al.*, An eclipsing 8.56 minute orbital period mass-transferring binary, *arXiv e-prints*, [arXiv:2601.07925 \(2026\)](#), [arXiv:2601.07925 \[astro-ph.SR\]](#).
- [68] K. B. Burdge *et al.*, Orbital Decay in an Accreting and Eclipsing 13.7 Minute Orbital Period Binary with a Luminous Donor, *Astrophysical Journal* **953**, L1 (2023), [arXiv:2303.13573 \[astro-ph.SR\]](#).
- [69] E. Roebber, R. Busicchio, A. Vecchio, C. J. Moore, A. Klein, V. Korol, S. Toonen, D. Gerosa, J. Goldstein, S. M. Gaebel, and T. E. Woods, Milky Way Satellites Shining Bright in Gravitational Waves, *Astrophysical Journal* **894**, L15 (2020), [arXiv:2002.10465 \[astro-ph.SR\]](#).

- ph.GA].
- [70] G. Ramsay, M. J. Green, T. R. Marsh, T. Kupfer, E. Breedt, V. Korol, P. J. Groot, C. Knigge, G. Nelemans, D. Steeghs, P. Woudt, and A. Aungwerojwit, Physical properties of AM CVn stars: New insights from Gaia DR2, *A&A* **620**, A141 (2018), arXiv:1810.06548 [astro-ph.SR].
- [71] A. Kosakowski, M. Dorsch, W. R. Brown, T. Kupfer, F. Ben Daya, and M. Kilic, A New LISA-detectable Type Ia Supernova Progenitor in the Southern Sky: SMSS J1138-5139, *Astrophysical Journal* **987**, 205 (2025), arXiv:2411.19391 [astro-ph.SR].
- [72] S. Sengupta and R. E. Taam, Theoretical Spectra of the AM Canum Venaticorum Binary System SDSS J0926+3624: Effects of Irradiation onto the Donor Star, *Astrophysical Journal* **739**, 34 (2011), arXiv:1107.1444 [astro-ph.HE].
- [73] K. B. Burdge *et al.*, General relativistic orbital decay in a seven-minute-orbital-period eclipsing binary system, *Nature* **571**, 528 (2019), arXiv:1907.11291 [astro-ph.SR].
- [74] J. Chakraborty *et al.*, Expanding the Ultracompacts: Gravitational-wave-driven Mass Transfer in the Shortest-period Binaries with Accretion Disks, *Astrophysical Journal* **977**, 262 (2024), arXiv:2411.12796 [astro-ph.HE].
- [75] K. B. Burdge, M. W. Coughlin, J. Fuller, D. L. Kaplan, S. R. Kulkarni, T. R. Marsh, E. C. Bellm, R. G. Dekany, D. A. Duev, M. J. Graham, A. A. Mahabal, F. J. Masci, R. R. Laher, R. Riddle, M. T. Soumagnac, and T. A. Prince, An 8.8 Minute Orbital Period Eclipsing Detached Double White Dwarf Binary, *Astrophysical Journal* **905**, L7 (2020), arXiv:2010.03555 [astro-ph.SR].
- [76] K. B. Burdge *et al.*, A Systematic Search of Zwicky Transient Facility Data for Ultracompact Binary LISA-detectable Gravitational-wave Sources, *Astrophysical Journal* **905**, 32 (2020), arXiv:2009.02567 [astro-ph.SR].
- [77] W. R. Brown, M. Kilic, A. Bédard, A. Kosakowski, and P. Bergeron, A 1201 s Orbital Period Detached Binary: The First Double Helium Core White Dwarf LISA Verification Binary, *Astrophysical Journal* **892**, L35 (2020), arXiv:2004.00641 [astro-ph.SR].
- [78] K. B. Burdge, J. Fuller, E. S. Phinney, J. van Roestel, A. Claret, E. Cukanovaite, N. P. Gentile Fusillo, M. W. Coughlin, D. L. Kaplan, T. Kupfer, P.-E. Tremblay, R. G. Dekany, D. A. Duev, M. Feeney, R. Riddle, S. R. Kulkarni, and T. A. Prince, Orbital Decay in a 20 Minute Orbital Period Detached Binary with a Hydrogen-poor Low-mass White Dwarf, *Astrophysical Journal* **886**, L12 (2019), arXiv:1910.11389 [astro-ph.SR].
- [79] L. O. McNeill and R. Hirai, Tidal Heating in Detached Double White Dwarf Binaries, *Astrophysical Journal* **992**, 154 (2025), arXiv:2507.21821 [astro-ph.SR].
- [80] W. R. Brown, M. Kilic, A. Kosakowski, and A. Gianninas, The ELM Survey. IX. A Complete Sample of Low-mass White Dwarf Binaries in the SDSS Footprint, *Astrophysical Journal* **933**, 94 (2022), arXiv:2207.02998 [astro-ph.SR].
- [81] M. Barrientos, M. Kilic, W. R. Brown, F. B. Daya, A. Bédard, T. Littenberg, T. Kupfer, and S. Sahu, Precise Parameters for Two LISA Sources, *Astrophysical Journal* **991**, 65 (2025), arXiv:2508.04156 [astro-ph.SR].
- [82] M. Kilic, W. R. Brown, A. Bédard, and A. Kosakowski, The Discovery of Two LISA Sources within 0.5 kpc, *Astrophysical Journal* **918**, L14 (2021), arXiv:2108.08324 [astro-ph.SR].
- [83] E. Stringer, T. Kupfer, and M. Dorsch, Detailed follow up studies of three ultracompact sdB binaries, *Bulletin de la Societe Royale des Sciences de Liege* **92**, 11283 (2023), arXiv:2303.05523 [astro-ph.SR].
- [84] Y. Götzberg, V. Korol, A. Lamberts, T. Kupfer, K. Breivik, B. Ludwig, and M. R. Drout, Stars Stripped in Binaries: The Living Gravitational-wave Sources, *Astrophysical Journal* **904**, 56 (2020), arXiv:2006.07382 [astro-ph.SR].
- [85] A. Kosakowski, W. R. Brown, M. Kilic, T. Kupfer, A. Bédard, A. Gianninas, M. A. Agüeros, and M. Barrientos, The ELM Survey South. II. Two Dozen New Low-mass White Dwarf Binaries, *Astrophysical Journal* **950**, 141 (2023), arXiv:2305.03079 [astro-ph.SR].
- [86] M. W. Coughlin, K. Burdge, E. S. Phinney, J. van Roestel, E. C. Bellm, R. G. Dekany, A. Delacroix, D. A. Duev, M. Feeney, M. J. Graham, S. R. Kulkarni, T. Kupfer, R. R. Laher, F. J. Masci, T. A. Prince, R. Riddle, P. Rosnet, R. Smith, E. Serabyn, and R. Walters, ZTF J1901+5309: a 40.6-min orbital period eclipsing double white dwarf system, *MNRAS* **494**, L91 (2020), arXiv:2004.00456 [astro-ph.HE].
- [87] V. Chandra, H.-C. Hwang, N. L. Zakamska, B. T. Gänsicke, J. J. Hermes, A. Schwöpe, C. Badenes, G. Tovmassian, E. B. Bauer, D. Maoz, M. R. Schreiber, O. F. Toloza, K. P. Inight, H.-W. Rix, and W. R. Brown, A 99 minute Double-lined White Dwarf Binary from SDSS-V, *Astrophysical Journal* **921**, 160 (2021), arXiv:2108.11968 [astro-ph.SR].
- [88] P. F. L. Maxted, T. R. Marsh, C. K. J. Moran, and Z. Han, The triple degenerate star WD 1704+481, *MNRAS* **314**, 334 (2000), arXiv:astro-ph/0001212 [astro-ph].
- [89] K. Deshmukh, E. B. Bauer, T. Kupfer, and M. Dorsch, Modelling the AM CVn and double detonation supernova progenitor binary system CD-30°11223, *MNRAS* **527**, 2072 (2024), arXiv:2310.01293 [astro-ph.SR].
- [90] J. J. M. in't Zand, R. Cornelisse, and M. Méndez, On the nature of two low-dot{M} X-ray bursters: 1RXS J170854.4-321857 and 1RXS J171824.2-402934, *A&A* **440**, 287 (2005), arXiv:astro-ph/0505516 [astro-ph].
- [91] S. Prodan and N. Murray, On the Dynamics of Ultra Compact X-Ray Binaries: 4U 1850-087, 4U 0513-40, and M15 X-2, *Astrophysical Journal* **798**, 117 (2015), arXiv:1411.0368 [astro-ph.HE].